Fermi National Accelerator Laboratory

FERMILAB-Conf-77/62-EXP
7000.260

COMPARISON OF HADRON JETS PRODUCED BY π^- AND p BEAMS ON HYDROGEN AND ALUMINUM TARGETS*

C. Bromberg, G. Fox, R. Gomez, J. Pine, S. Stampke, and K. Yung
California Institute of Technology, Pasadena, California 91125

and

S. Erhan, E. Lorenz, M Medinnis, J Rohlf, and P. Schlein
University of California, Los Angeles, California 90024

and

V. Ashford, H. Haggerty, R. Juhala, E. Malamud, and S. Mori
Fermi National Accelerator Laboratory, Batavia, Illinois 60510

and

R. Abrams, R. Delzenero, H. Goldberg, F. Lopez,
S. Margulies, D. McLeod, J. Solomon, and R. Stanek
University of Illinois at Chicago Circle, Chicago, Illinois 60680

and

A. Dzierba and W. Kropac
Indiana University, Bloomington, Indiana 47401

August 1977

*Presented by E. Malamud at the VIII International Symposium on Multiparticle Dynamics, Kaysersberg, France, June, 1977.

FERMILAB-Conf-77/62-EXP
UCLA-1110
IUHEE-13
UICC-77-2

COMPARISON OF HADRON JETS PRODUCED BY π^- AND p BEAMS ON HYDROGEN AND ALUMINUM TARGETS*

C. Bromberg, G. Fox, R. Gomez, J. Pine, S. Stampke, and K. Yung
California Institute of Technology, Pasadena, California 91125

and

S. Erhan, E. Lorenz,† M. Medinnis, J. Rohlf, and P. Schlein
University of California, Los Angeles, California 90024

and

V. Ashford, H. Haggerty, R. Juhala,†† E. Malamud, and S. Mori
Fermi National Accelerator Laboratory, Batavia, Illinois 60510

and

R. Abrams, R. Delzenero, H. Goldberg, F. Lopez,
S. Margulies, D. McLeod, J. Solomon, and R. Stanek
University of Illinois at Chicago Circle, Chicago, Illinois 60680

and

A. Dzierba and W. Kropac†††
Indiana University, Bloomington, Indiana 47401

ABSTRACT

We present results from an experiment studying the production of single charged particles and jets (groups of particles) with high p_t (transverse momentum) produced in 200 GeV interactions using a calorimeter triggered multiparticle spectrometer. Results are presented on the coplanarity, momentum distribution of charged particles, and cross-sections for liquid hydrogen and aluminum targets and for incident pions and protons. These results give strong support to a simple quark-quark scattering model.

I. INTRODUCTION

This is a report on results from Fermilab experiment E-260, a study of hadron jets produced in hadron-hadron collisions using a calorimeter triggered multiparticle spectrometer. The spectrometer is located in a building at the end of the West branch of the M6 beam in the meson area. The original motivation for this experiment was the observation[1] of unexpectedly large inclusive cross-sections at high p_t. Subsequent observations of jets in e^+e^- → hadrons at SPEAR[2] and jet like structure opposite a high p_t trigger and same side correlations at the ISR[3] gave further impetus to this study.

Various hard scattering models have been formulated to describe high p_t data. The most frequently discussed at present are the quark-quark scattering model[4] as represented schematically in Fig. 1, and the constituent interchange model.[5]

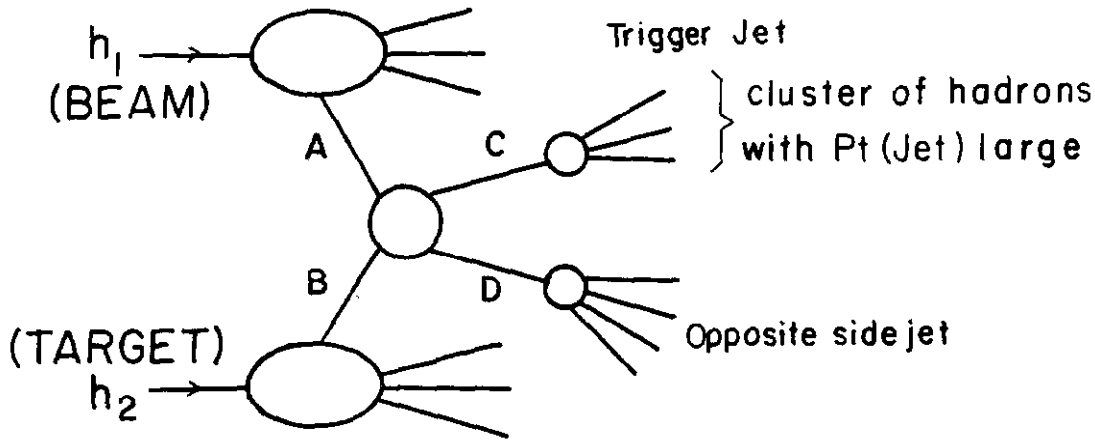

Figure 1

In such models jets are the result of the materialization or fragmentation of the scattered partons (quarks) into hadrons and appear as a cluster of charged and neutral particles with limited transverse momentum relative to their common axis and carrying the (large) p_t of their parent parton. The overall transverse momentum will be balanced by either an opposite side jet or single high p_t particle thus giving the event a coplanar structure. Because the jets result from a binary collision of partons each of which carries only a fraction of the incident momenta, the resulting jets will not be necessarily colinear in the center-of-mass system. A universality of hard scattering suggests that jets will have a structure similar to that observed in lepton or e^+e^- produced jets.

A crucial test of constituent models is to compare data with different incident hadrons. We are limited statistically in our ability to do this with our Beryllium target test data[6] but now we have sufficient statistics to compare incident p, π^-, π^+. We will also later be able to say something qualitative about $\bar{p}$, K^+, and K^- induced jets.

The main new aspect of this talk over what is already published from our experiment[6] will be this incident hadron comparison as well as the A-dependence, obtained from two targets: hydrogen and aluminum.

The experiment will be described (Section II), some details on the quality and quantity of the data given (III) and then the results presented will be divided into three categories:

(IV) Coplanarity

(V) Jet Structure

(VI) Cross-Sections

II. DESCRIPTION OF THE APPARATUS

A plan view of the experiment is shown in Fig.2.

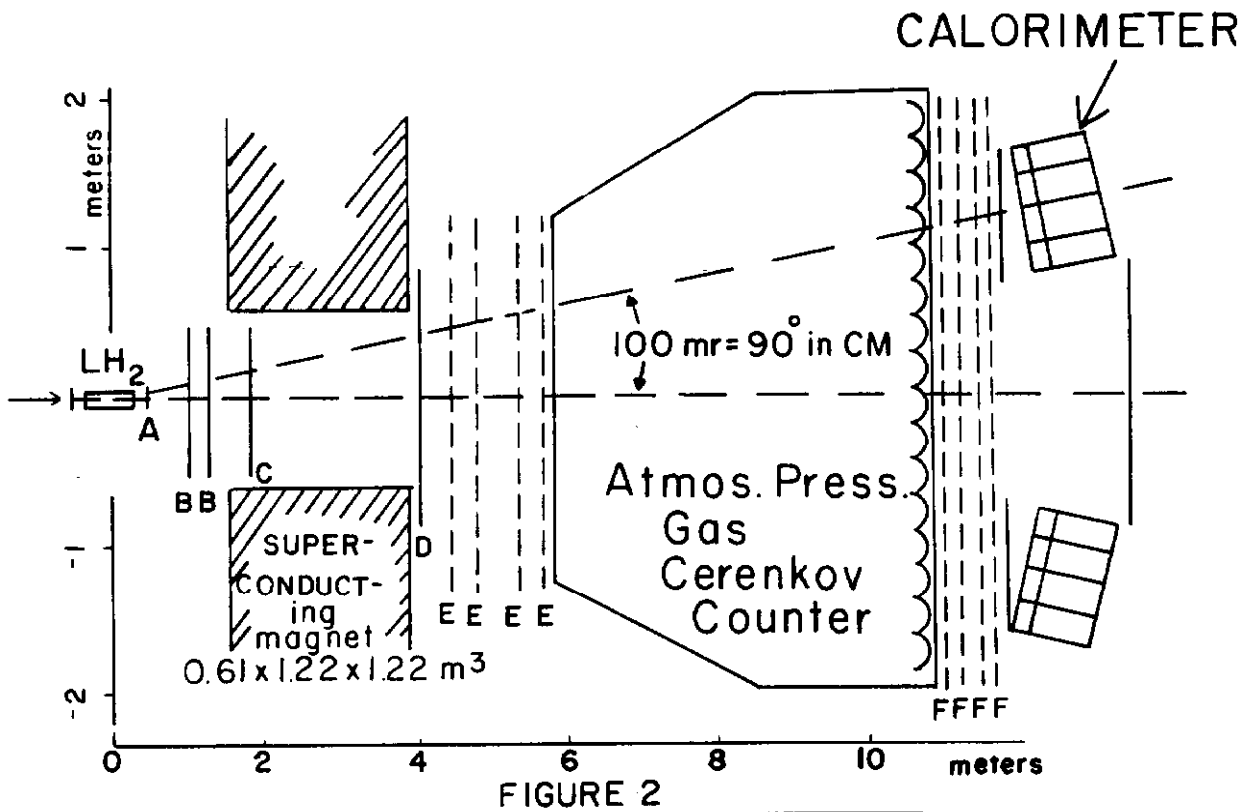

FIGURE 2

ABCD: MWPC 1-4.6 mm
EF: Spark Chambers, x, y, u,
up to 30 Sparks/plane

The hadrons in the incident beam[8] (M6 West) are tagged ($\pi^{\pm}$, $K^{\pm}$, p, $\bar{p}$) by four beam Cerenkov counters. Most of the data was taken at an incident momentum of 200 GeV/c and a flux of 2×10^6/second, during a two second spill, approximately 4 times/minute.

The spectrometer magnet is superconducting with a maximum $\int Bdl$ of 25 kg-m, although in this experiment we ran at half this value to minimize p_t smearing of the trigger. Track reconstruction in front of the magnet is done entirely with MWPC's; behind the magnet is a combination of large MWPC's and magnetostrictive spark chambers. The proportional chambers are used to make "roads" in the track reconstruction program for the higher resolution spark chambers. The multicelled gas Cerenkov counter is used for final state particle identification; analyses using this information are in progress and will be reported at a later time.

Two large modular calorimeters,[9] placed at approximately 90° in the center-of-mass are used for triggering on high p_t events. Since they are a crucial part of the experiment for both triggering and reconstruction of the jets, they will be described in more detail.

Figure 3 shows one of the two calorimeters.

CALORIMETER STRUCTURE

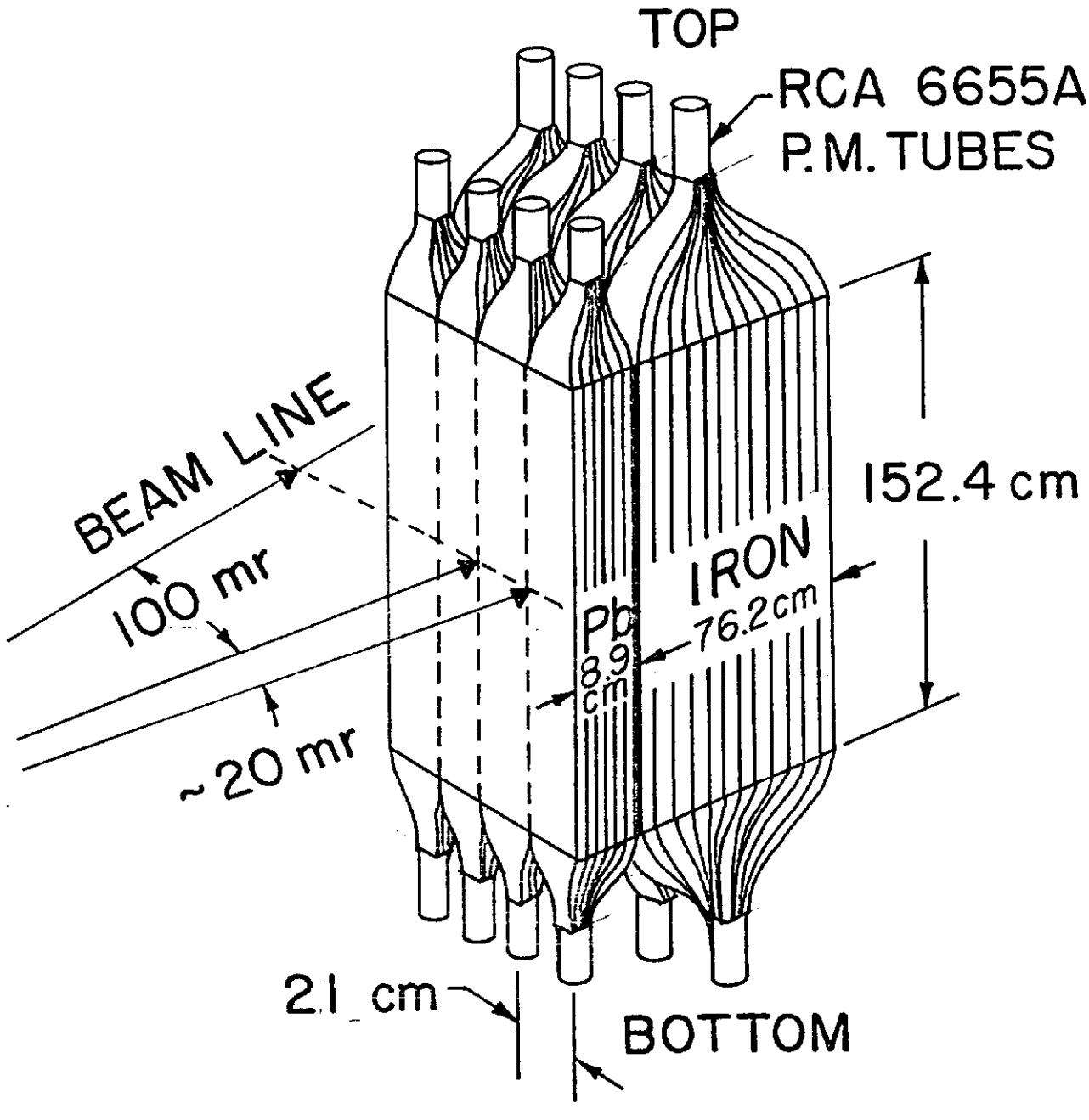

FIGURE 3

Each calorimeter is divided into 4 modules; each module contains a front, lead-scintillator sandwich shower counter, and a back iron-scintillator hadron cascade section. By using the ratio of the top and bottom phototube pulse heights, the mean vertical position of the particles entering the module can be determined to ±10 cm (at E = 25 GeV).

Table I gives some of the parameters of the calorimeter:

TABLE I

E-260 CALORIMETER PARAMETERS

Detector	Material	Total Thickness	Radiation Lengths	Absorption Lengths	σ, Energy Resolution
Photon	Pb-Scint.	8.5 cm	15	0.5	$\frac{0.33}{\sqrt{E}}$ GeV$^{-1/2}$
Hadron	Fe-Scint.	76 cm	43	4.5	$\frac{1.03}{\sqrt{E}}$ GeV$^{-1/2}$

The calorimeter has good lepton-hadron separation, done by comparing the pulse height from the lead and iron sections.

III. DESCRIPTION OF THE DATA

The pulse heights in the 4 modules are attenuated relative to each other by an amount proportional to θ_{LAB} to give signals proportional to p_t. These are then combined into two different triggers:

1) Single particle trigger, with p_t in any one of the 4 modules (on either side) greater than the trigger bias, (set at 2 and 3 GeV/c), and

2) Jet trigger, with the analog sum (or total p_t) of the 4 modules (on either side) greater than the trigger bias (set at 3 and 4 GeV/c).

In addition we recorded simultaneously a sample of unbiased total inelastic cross-section triggers ("interacting beam") which only required a beam interaction (except small angle scatters) to trigger.

The high p_t triggers are illustrated by the events shown in Fig. 4.

The p_t measured by the calorimeter modules shown in Fig. 4 includes both charged and neutral particles. In Fig. 4a, the single charged particle trigger has a p_t of 3.03 GeV/c compared to 3.8 GeV/c measured in the hadron portion of the second right-hand (looking downstream) module. In Fig. 4b a cluster of particles into the left-hand calorimeter triggered the spectrometer. Their total p_t in charged tracks measured by the spectrometer is 2.9 GeV/c compared to the sum of p_t's in the left-hand calorimeter of 5.3 GeV/c. The last event (Fig. 4c) shows ~6 GeV/c in the right-hand calorimeter and is unusual in that p_t is approximately balanced among the charged tracks (~2.5 GeV/c each side).

The magnet is run so that $\int Bdl = 12.5$ kg-m (1/2 field), and the p_t contribution of the magnet to each charged track is $\approx \pm .28$ GeV/c. The charged track efficiency is > 90% and the vertex efficiency is estimated to be (92 ± 3)%.

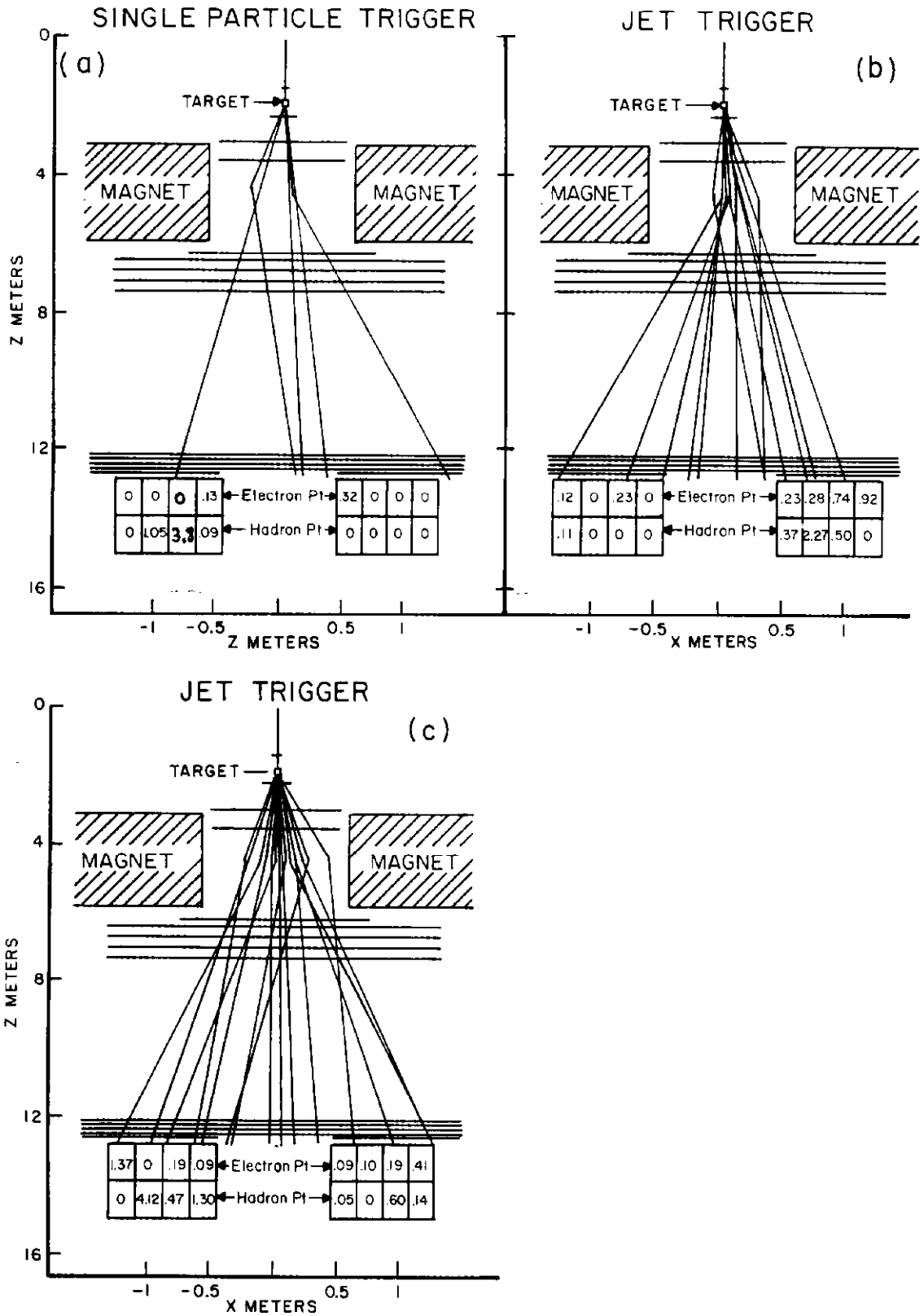
SINGLE PARTICLE TRIGGER
(a)
TARGET
MAGNET
MAGNET
Electron Pt
Hadron Pt
Z METERS
Z METERS
JET TRIGGER
(b)
TARGET
MAGNET
MAGNET
Electron Pt
Hadron Pt
X METERS
JET TRIGGER
(c)
TARGET
MAGNET
MAGNET
Electron Pt
Hadron Pt
Z METERS
X METERS

FIGURE 4

What is a jet? We use an empirical definition of a jet based on our apparatus: a jet is a cluster of particles with high p_t hitting our calorimeter. There are three components to this cluster: charged, electromagnetic neutral, and hadronic neutral. We require the jet vector, the vector sum of these components, to hit a fiducial area in the center of the calorimeter. The calorimeter acceptance for jets with properties described in Section I is discussed in Ref. 6.

There are a number of problems with this jet definition. A jet associated particle can miss the calorimeter, thus changing the magnitude and direction of the jet vector. In some cases the direction will change enough to move the jet vector from outside the fiducial area into the fiducial area or vice-versa, thus changing the cross-section. Another problem is a non-jet associated particle hitting the calorimeter, thus adding to the total p_t. These uncertainties in the cross-section will be made somewhat more quantitative in Section V.

The three components of the jet are determined as follows. The charged particles are determined by the spectrometer, with accuracy $\Delta p/p = .07\ p$ (GeV/c) percent. The electromagnetic and hadronic neutrals are determined with an energy resolution given in Table I above.

To get a feeling for the relative accuracy of the different jet components we describe a typical jet with $p_t = 5$ GeV/c produced at $\theta_{LAB} = 100$ mrad (90^o in c.m. at 200 GeV) so $E_{jet} = 50$ GeV. Charged particles take ~55% of the energy and $< n_c > \sim 2.5$.

A typical charged track of 10 GeV will be determined with a precision of $\leq$ 1%. The energy of a 10 GeV e.m. neutral is known to ~10% and a cleanly observed 10 GeV hadronic neutral would be known to ~30%. However, the actual resolution for hadronic neutrals is worse than that because they are found by subtraction:

$$E_{hn} = E_{\text{pulse ht}} - E_{e.m.} - E_{chg.}$$

The neutral energy estimate is very sensitive to fluctuations in the calorimeter response to charged hadrons and so we only accept a neutral if a series of rather strict requirements are met. The neutral determination is done separately for each module (four electron and four hadron per calorimeter). From the reconstructed tracks (assumed to be hadrons), the expected calorimeter pulse heights are calculated. These pulse heights are converted to an energy, E_T, and vertical position, y_t. This procedure uses the mean shower shapes and includes corrections for leakage and the electron module response to hadrons. The observed calorimeter pulse heights in each module correspond to an energy, E_m, and vertical position, y_m. Our neutral particle candidate has parameters E_n, y_n determined by

$$E_n = E_m - E_t$$

$$E_n y_n = E_m y_m - E_t y_t$$

We accept a <u>neutral</u> if

(a) $E_m \geq 1.0$ GeV, and

(b) $|y_m| \leq 0.7$ m.

In addition, we eliminate those rare cases where a charged hadron deposits most of its energy in the electron module and a little in the hadron module behind it.

Additional conditions on an electromagnetic neutral are:

(a) $\frac{E_t}{E_m} \leq 3$, and

(b) $\frac{E_t}{E_m} \leq 1/2$ or $\left|Y_t - Y_m\right| \geq 15$ cm.

Additional conditions on a hadronic neutral are:

(a) No charged particle entering the center 15 cm (of the 21 cm wide) hadron module, and

(b) $\frac{E_t}{E_m} \leq 4/3$, and

(c) If charged particles enter the outer edges of the module then more restrictive cuts are placed on $\frac{E_t}{E_m}$ and $\left|y_t - y_m\right|$.

The hadronic neutral component includes, in the present analysis, track finding inefficiencies and non-vertex associated charged tracks (e.g., K^o, Λ^o decays) as well as real neutral hadrons (K_L^o and neutrons). This component has the biggest uncertainty. If we were to use the total calorimeter pulse height to measure the jet cross-section we would overestimate it because we are measuring a steep spectrum with a poor resolution device (shown in Fig. 24).

The large acceptance of our apparatus is illustrated in Fig. 5. The acceptance is nearly 100% in the forward hemisphere.

The diagonal lines show the kinematic boundaries of the four calorimeter modules making up the trigger. The magnetic field causes some smearing at these boundaries; this problem will be discussed further in Section V.

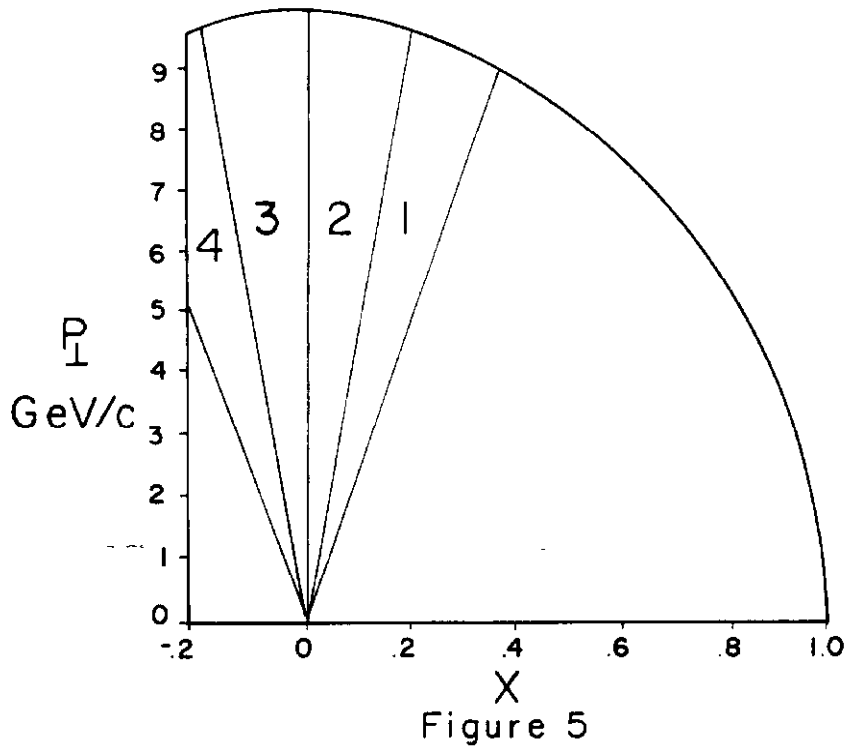

Figure 5

In Table II we summarize our data sample:

TABLE II

E-260 DATA SUMMARY

Target	P_{beam} (GeV/c)	Triggers (All Types)	Jet Trigger Thresholds GeV/c	Calorimeter Centered At θ_{LAB}	At θ_{cm}	Data Taken
Be	200±	100K	3, 4, 4.5	80 mrad	79°	Jan. 1976
H_2 (Al)	200±	870K	3, 4	100 mrad	92°	June-Sept 1976
	130±	130K		120 mrad	90°	

This report will discuss results from a preliminary analysis of ~270K (or about 30%) of the 200 GeV/c ± H_2 (Al) data. Some comparisons will be made with the already published and soon to be published Be data.[6] Besides the physics difference of having the calorimeters centered at a different angle in the Be and H_2 runs there are also analysis differences. A different (and better) vertex algorithm was used in the H_2 data.

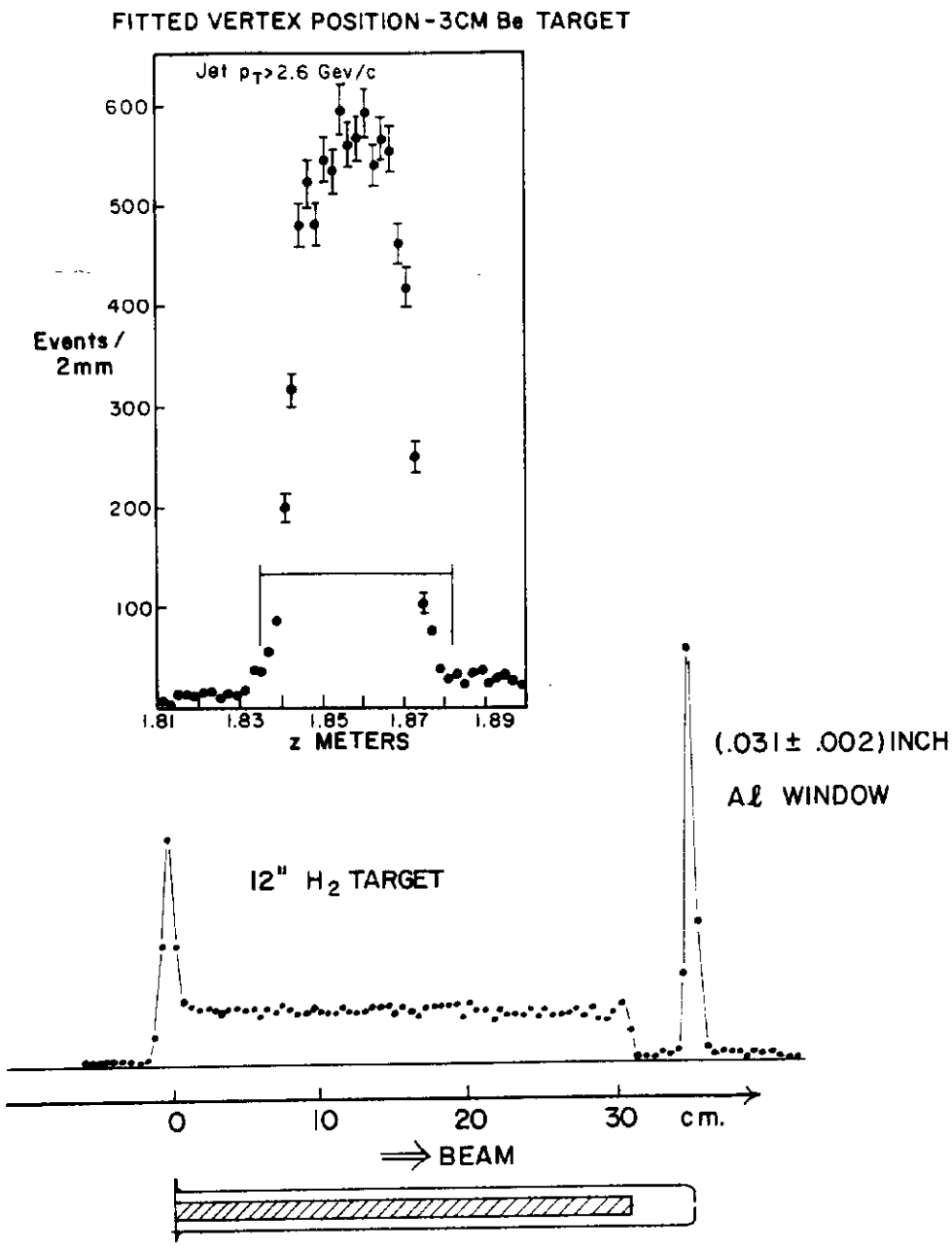

FIGURE 6

This was necessitated by the extended target. A third difference was the way in which hadronic neutrals were determined. The vertex distributions for the two runs, Be and H_2 (Al), are shown in Fig. 6.

The vertex resolution is better than ±5 mm so that there is a clear separation of the hydrogen from the aluminum vacuum jacket and we can obtain the A-dependence of the cross-sections given in Section VI.

For technical reasons the preliminary H_2 analysis was done with the omission of wide-angle tracks that miss the F-spark chamber station. (See Fig. 2). This lowers the multiplicity but part of the difference seen in Fig. 7 may be an A-dependent effect.

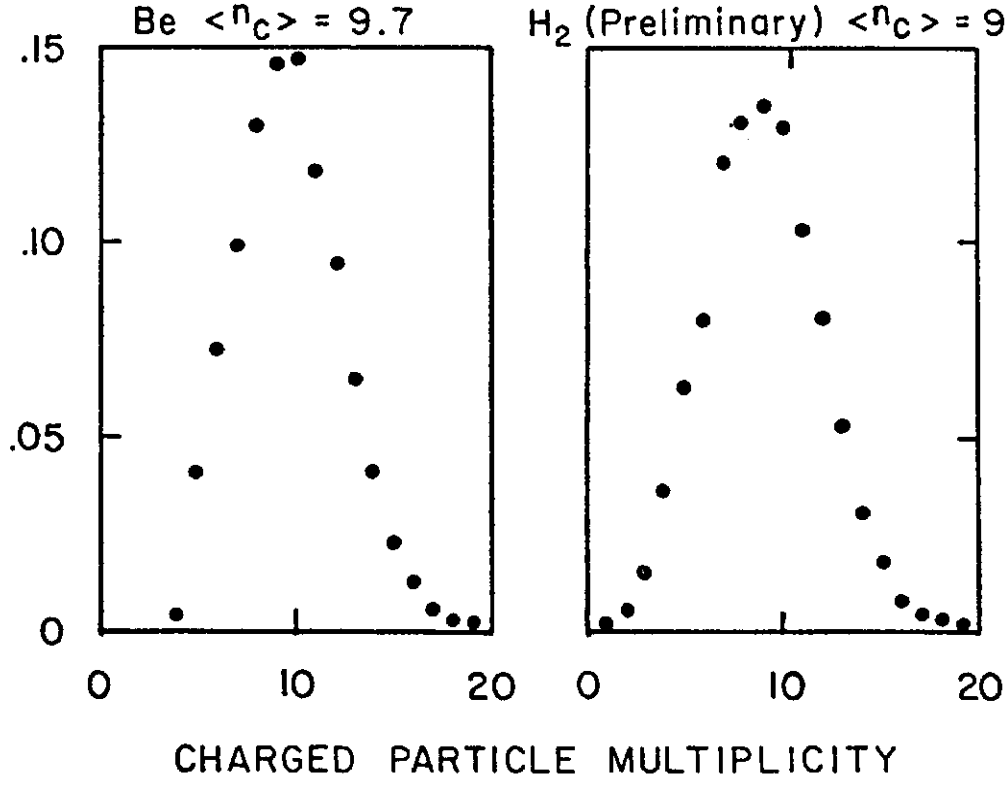

FIGURE 7

The multiplicities shown in Fig. 7 are for momentum analyzed tracks from the primary vertex. Some additional vertex associated tracks have large laboratory angles and do not go through the magnet. The total charged multiplicity before the magnet can be estimated from the number of hits in the B and C proportional chambers (see Fig. 2) and is about 14. This is a dramatic increase over the total charged multiplicity of 7.5 observed at this energy without a p_t selection.[10] The preliminary analysis of the hydrogen data reported here is based on an early version of the track-finding program. The data used in this report is being reprocessed along with the full statistics and both 200 and 130 GeV samples. But it is not expected that the results shown here will change significantly. The final processing will, of course, include the wide angle tracks, which will raise the multiplicity by 5 to 10% and modify the low z portion of the z distributions shown in Section V. Also non-vertex tracks will be found which may modify the hadronic neutral component and also allow us to investigate K^o and $\Lambda(\bar{\Lambda})$ production in the high p_t events.

IV. COPLANARITY

All constituent models for high p_t processes predict coplanar structure. Our dataare consistent with this prediction for both jet and single particle triggers.

We use the technique of sphericity analysis as introduced by the SPEAR group[2] to study jets in e^+e^- collisions, except that we work in the transverse plane as illustrated below (z is the beam direction).

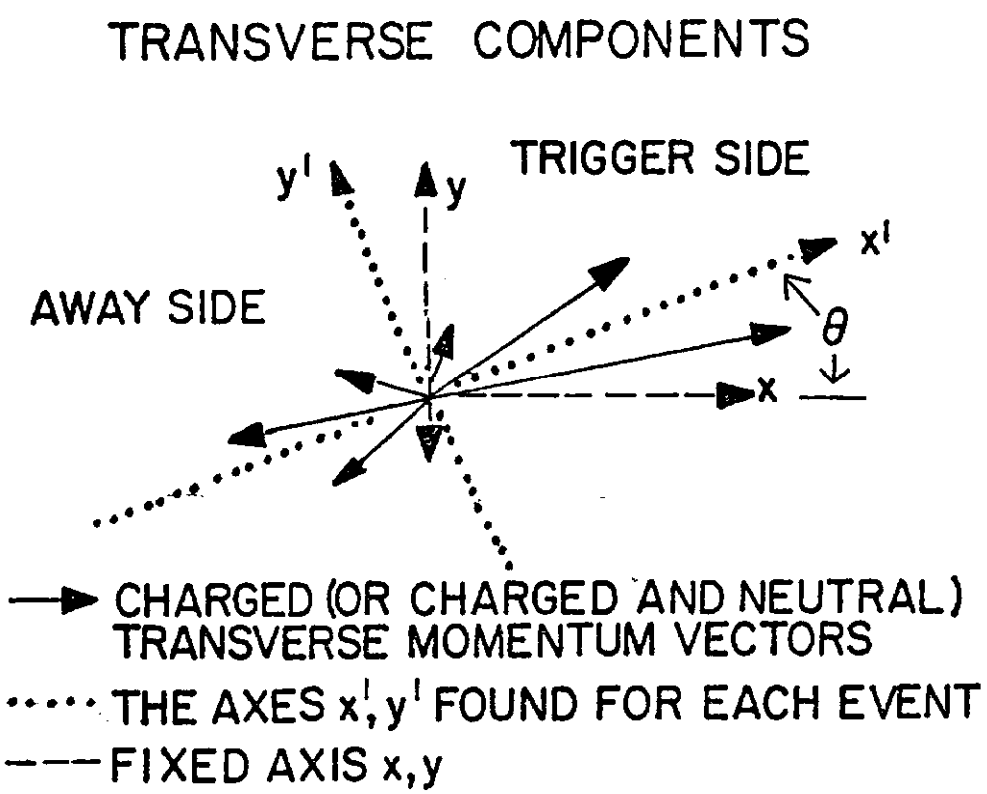

The axes x' and y' are found using:

$$R(\theta)\begin{pmatrix} \Sigma P_y^2 & -\Sigma P_x P_y \\ -\Sigma P_x P_y & \Sigma P_x^2 \end{pmatrix} R^T(\theta) = \begin{pmatrix} \lambda_1^2 & 0 \\ 0 & \lambda_2^2 \end{pmatrix}$$

where $R(\theta)$ is a two-dimensional rotation matrix. These axes maximize and minimize the rms momentum components respectively. The eigenvalues λ_1 and λ_2 are these rms components along y' and x', and we will use them as a test of the coplanarity of the events.

There is <u>one</u> set of principal axes determined for the whole event. It can be determined using only charged tracks, or can be determined using the charged and neutral particles. The results presented below on the values of λ_{max} and λ_{min} were found by using only charged particles. For the other results in the rest of this report the best jet axis was found using all the particles. Away side distributions in p_{in}, p_{out}, and z contain all charged particles with $|y_{cm}| < 1.0$. Trigger side distributions include only particles into the trigger side calorimeter.

Reference 6 discusses the comparison of λ_{max} and λ_{min} with values calculated by a simple Monte Carlo model. A summary of that comparison follows:

(1) $\lambda_{min} \propto \sqrt{n_c}$ which is what one would expect from uncorrelated momentum vectors that are independent of multiplicity.

(2) In a fireball model there is no preferred axis so $\lambda_{max} \approx \lambda_{min}$. However, the maximizing principal guarantees that $\lambda_{max} > \lambda_{min}$. So how significant are these results? The Monte Carlo calculation used the measured single particle spectrum to generate the transverse momentum of particles independently (without regard to conservation laws). This yielded $\lambda_{max} \approx 1.5$ to 2 times λ_{min}.

(3) The Monte Carlo generated λ_{max} increases with increasing multiplicity as $\sqrt{n_c}$ as expected from random walk.

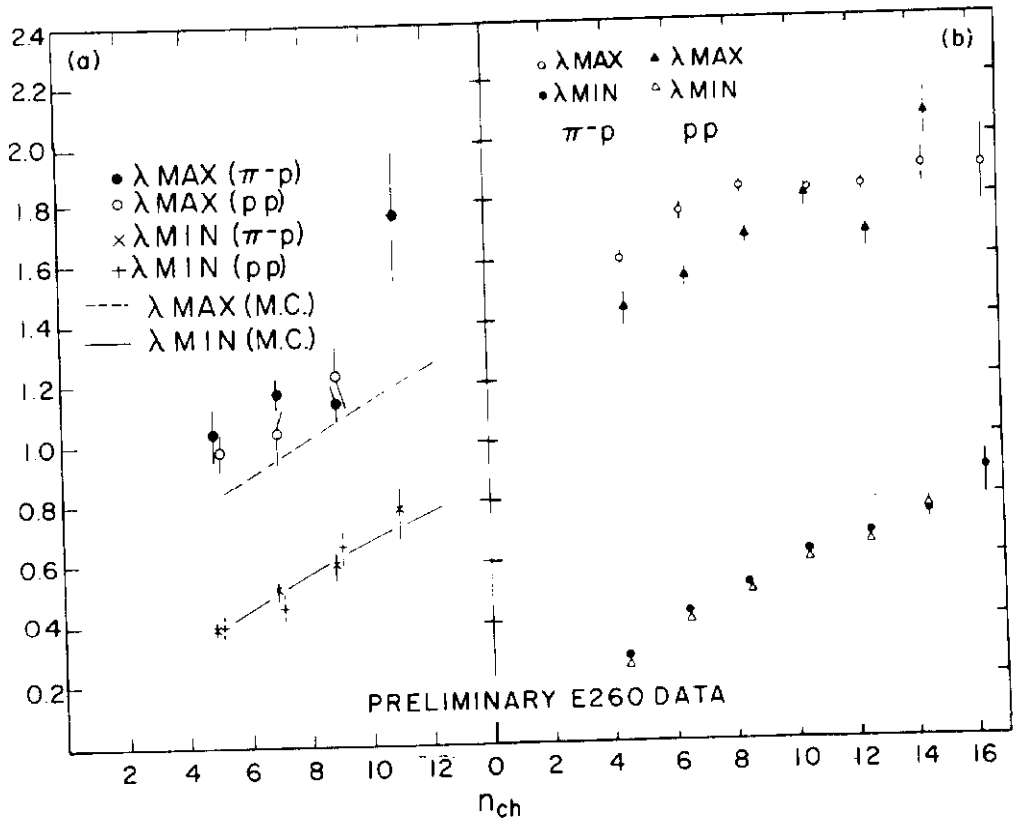

Figure 8

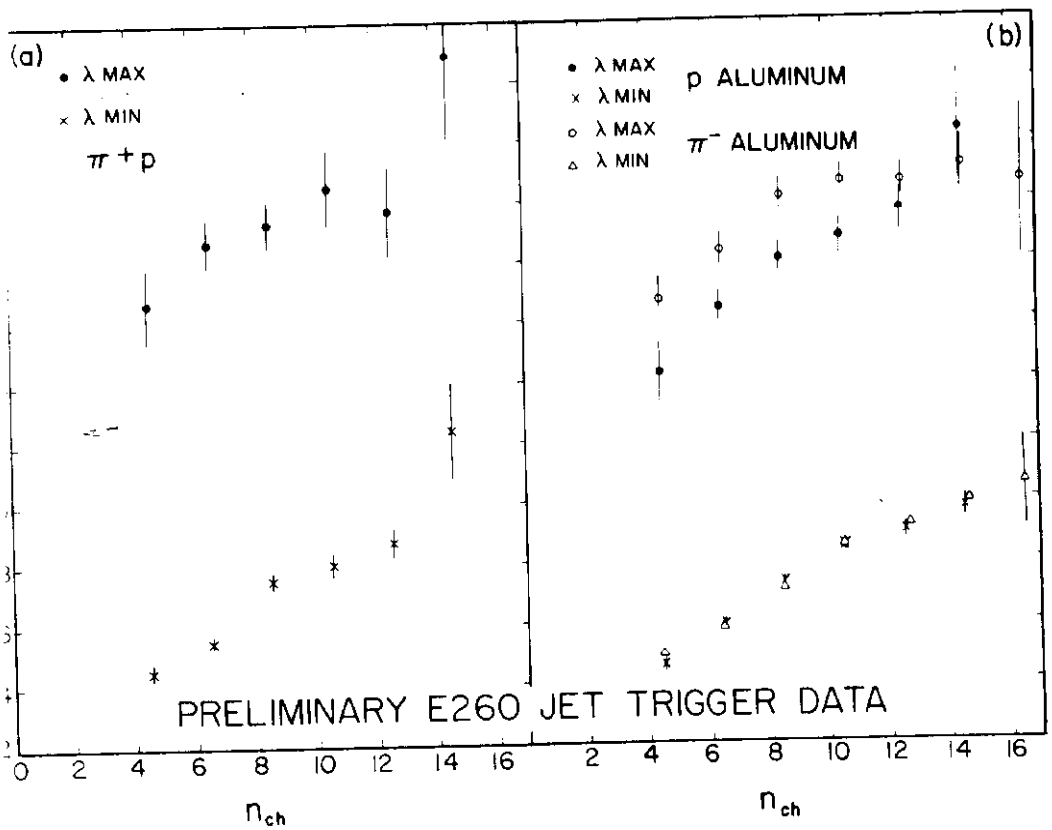

Figure 9

In Fig. 8a we compare the results of the Monte Carlo calculation with λ_{max} and λ_{min} as a function of n_c (total downstream charged multiplicity), determined from our interacting beam data. These values are calculated using only events in the interacting beam data with p_t jet $\geq$ 1.0 GeV/c. The calorimeter is not in the trigger; p_t jet is determined in the same way as in the analysis of the jet trigger data.

Figure 8b shows λ_{max} and λ_{min} as a function of charged particle multiplicity for jet trigger data with a jet momentum cut of $3 \leq p_t \leq 7$ GeV/c. Only data taken with a trigger bias of 4 GeV/c were used but events below threshold included. These comments apply to the rest of the figures in this and the next section (V).

In the low p_t interacting beam data the λ_{max} and λ_{min} agree reasonably well with the Monte Carlo calculation. In contrast the jet trigger data shows a λ_{min} roughly in agreement with the Monte Carlo calculation, but a λ_{max} that is strikingly larger, and also more constant with n_c than $\sqrt{n_c}$. This coplanar structure in the jet trigger events is similar to that found in the analysis of the Beryllium test data.

For completeness we show in Fig. 9a λ_{max} and λ_{min} for $\pi^+ p$ collisions and in Fig. 9b these parameters determined from our p-Al and π^--Al data. Both figures 8b and 9b appear to show a different dependence of λ_{max} on n_c for incident protons and pions.

Next we turn to distributions in p_{in} and p_{out}, the components along the principal axes (found using all the charged and neutral particles). These distributions are normalized so the total area under the graphs equals the charged multiplicity. On the away side a correction factor is obtained using the away side rapidity distributions shown in Fig. 10 and assuming they should be symmetric about 90°. (True only for a y=0 trigger). This procedure is probably incorrect for the $\pi^- p$ case. The correction (=2F/(F+B)) to the away side multiplicity is ~1.7.

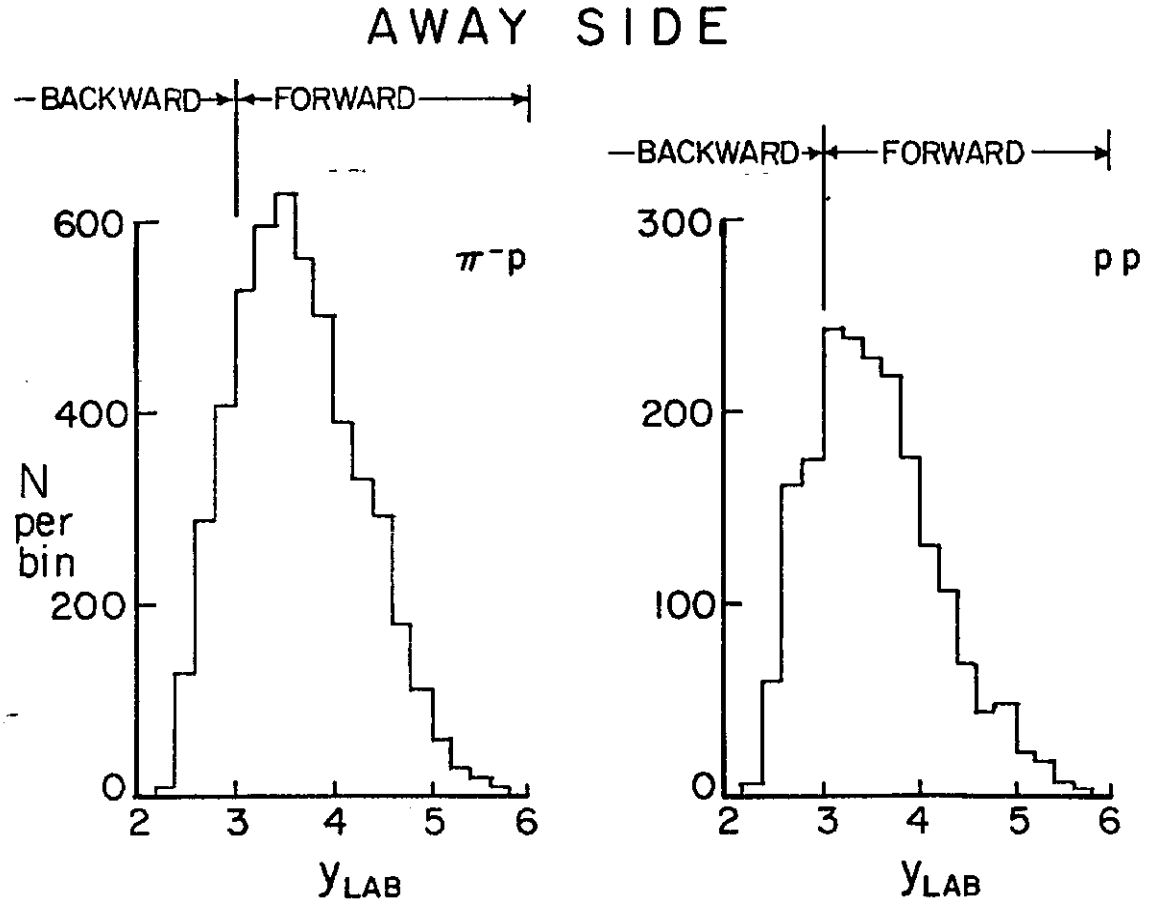

Figure 10

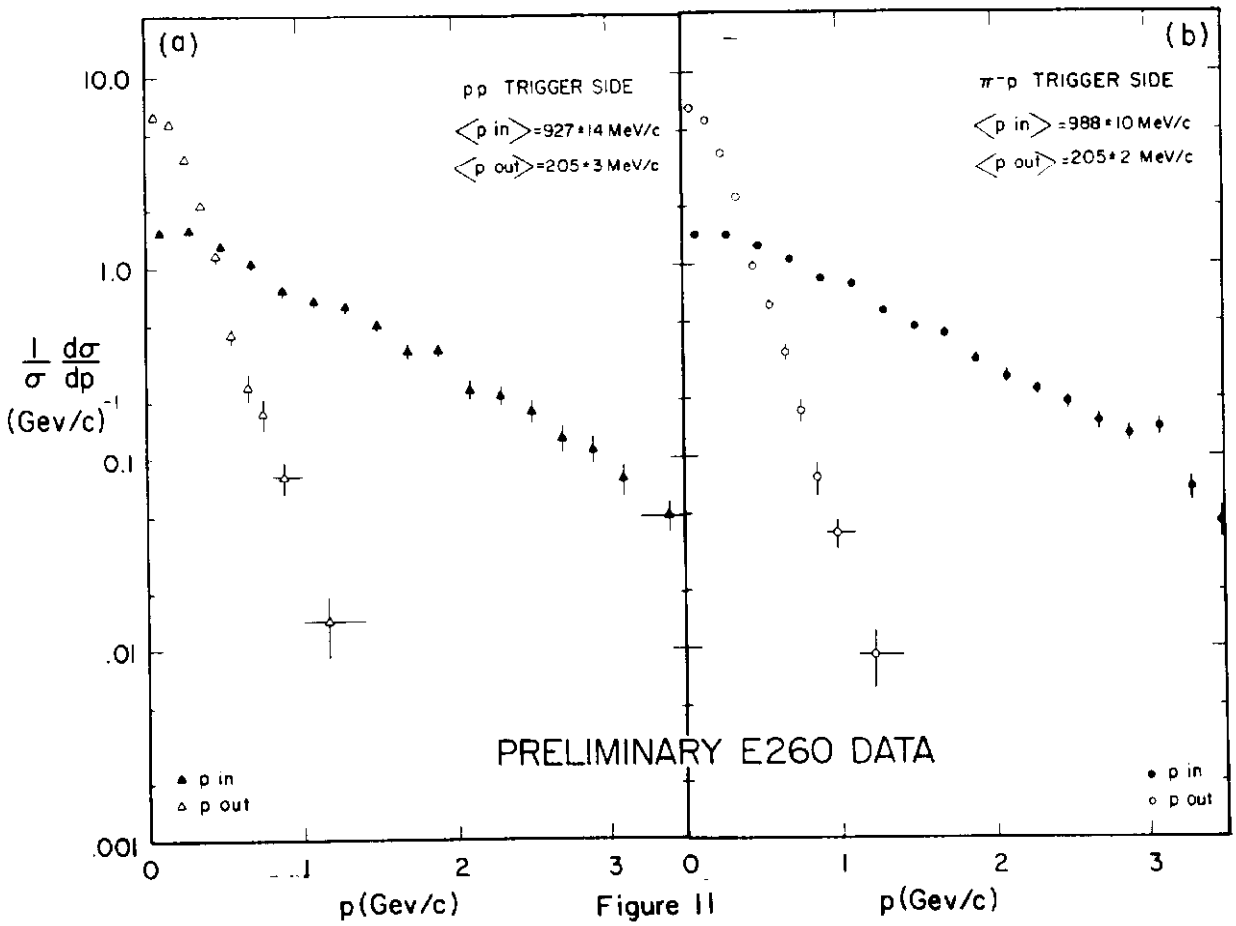

Figure 11

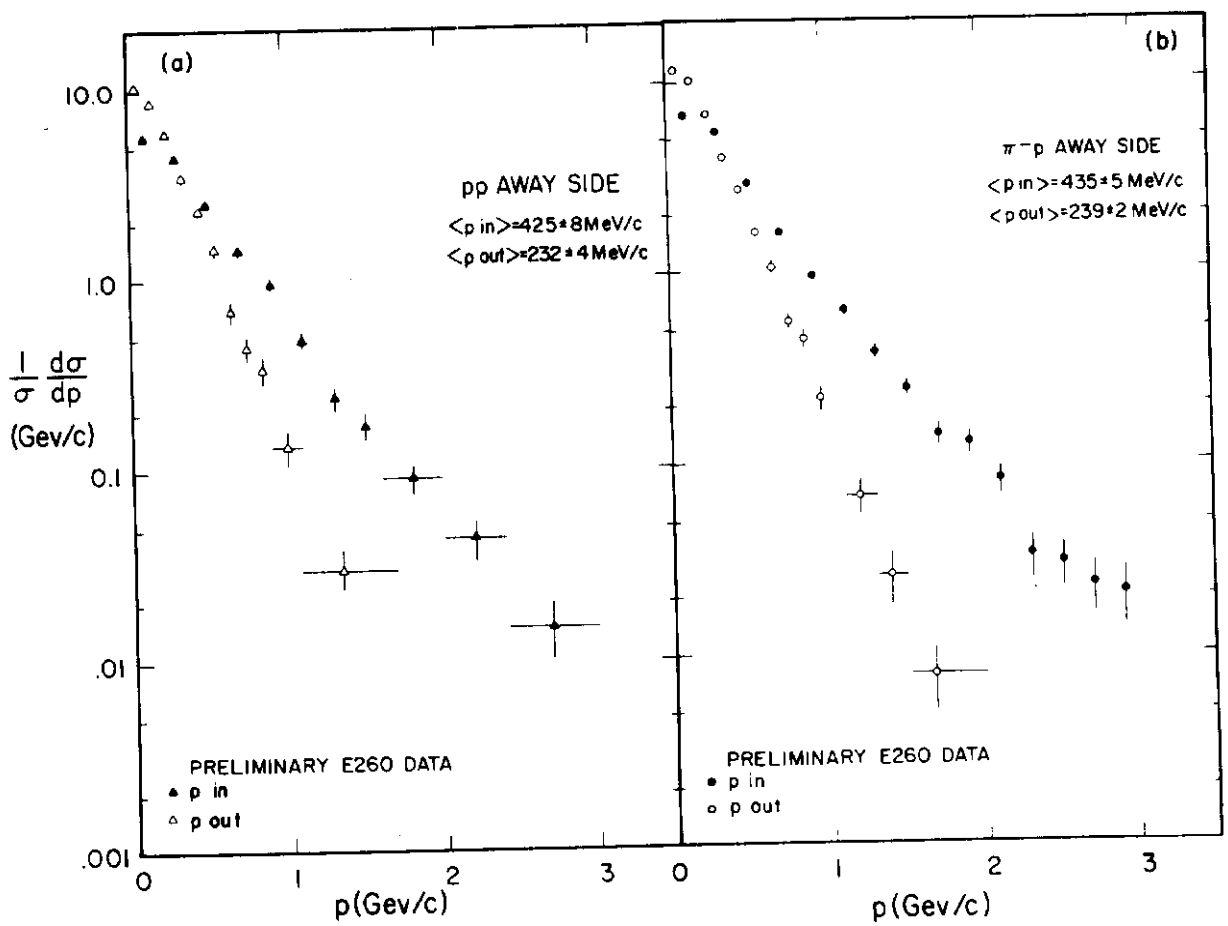

Figure 12

Normalized p_{in} and p_{out} distributions for the trigger and away sides are shown in figures 11 and 12. Distributions in p_{in} and p_{out} with an aluminum target are similar.

Another way to present these data (which are equivalent to azimuthal distributions) is to define a jet "shrinkage" shown in Fig. 13. The dotted lines in the figure are to guide the eye and approximate the trend of the $\pi^- p$ points. It can be seen that both trigger and away sides "shrink" at the same rate, within statistics.

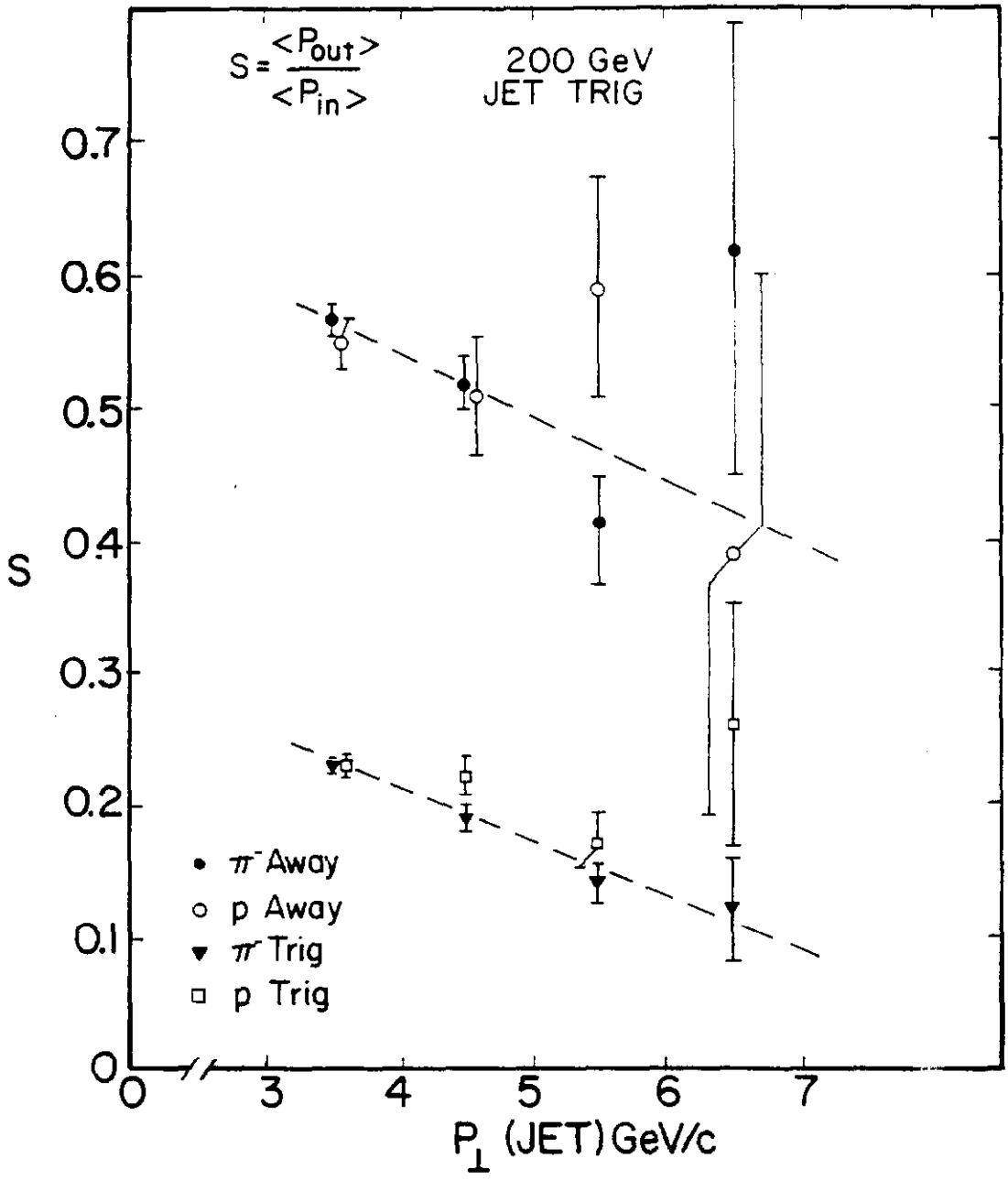

Figure 13

Our experiment has large azimuthal acceptance so our p_{out} is clear. It is sharply cut off on both trigger and away sides and has a mean ~200 MeV/c. P_{in} is much flatter and on the trigger side, is almost two orders of magnitude larger at 1 GeV/c.

Before concluding the discussion of coplanarity we present in Fig. 14 the away side p_{out} distribution for single particle triggers (p_t > 2 GeV/c). Here we do not use the principal axis but the direction defined by the trigger particle itself. These distributions are broader than the p_{out} distribution obtained from jet trigger data (Fig. 12) which is shown as dotted lines in Fig. 14 for comparison. Presumably this difference is due to the fact that the single particle does not coincide with the best jet direction (principal axis). The width of our single particle p_{out} distribution is similar to that observed at the ISR.[3]

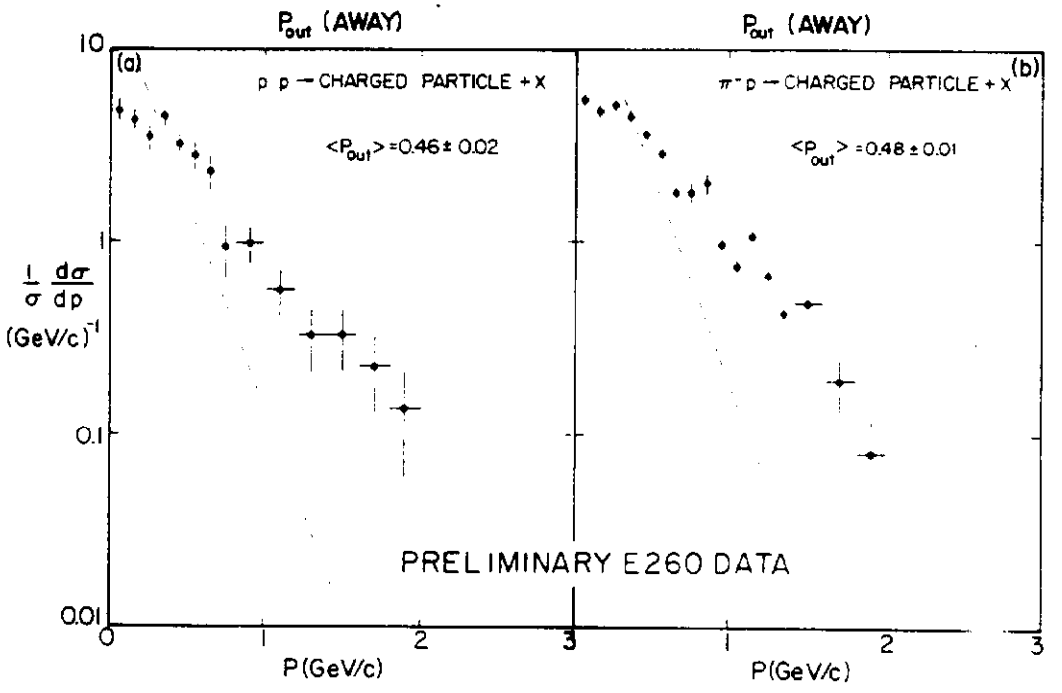

Figure 14

We return to the jet trigger data to make some additional comments. In Fig. 15 we show the away side transverse momentum. This includes all charged particles with $|y_{cm}| < 1.0$ plus whatever neutral particles are found in the away side calorimeter. We see the same momentum imbalance as observed in the Be data.

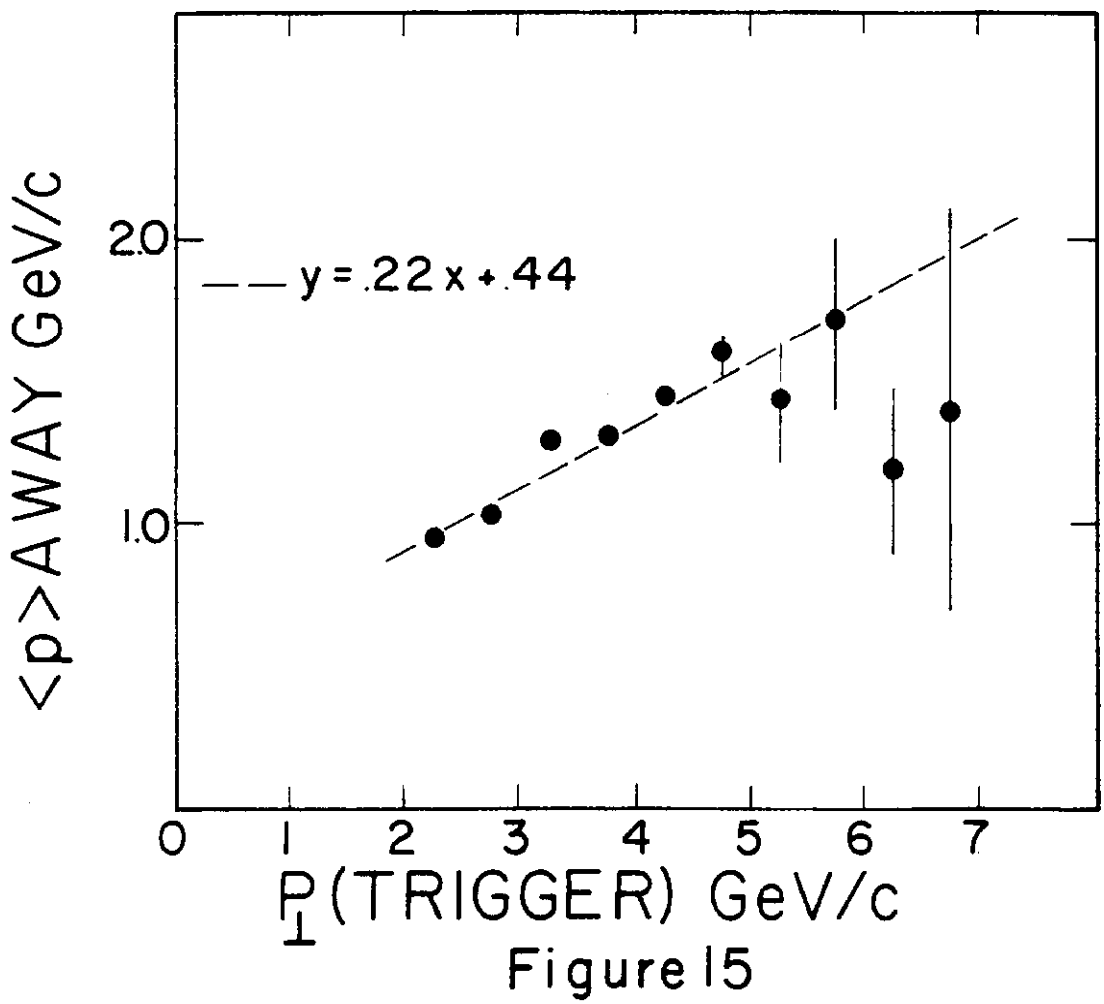

Figure 15

In Fig. 16 we show the negative of the mean of the vector sum of the transverse momentum of all forward charged particles ($y_{cm} > 1$) projected onto the principal axes as a function of the p_t of the trigger jet. This shows that the forward going system helps balance the trigger jet transverse momentum in agreement with the quark scattering picture in which the incident quarks have transverse momenta, k_t, and on the average the trigger selects events in which the k_t points in the trigger direction. The value of the forward p_t implies the width of the k_t distribution is of the order of 350 to 500 MeV/c, although there is still some uncertainty in track reconstruction in the very forward direction (near the beam). These data include 3 and 4 GeV/c trigger biases; there appears to be a threshold effect at 4 GeV/c.

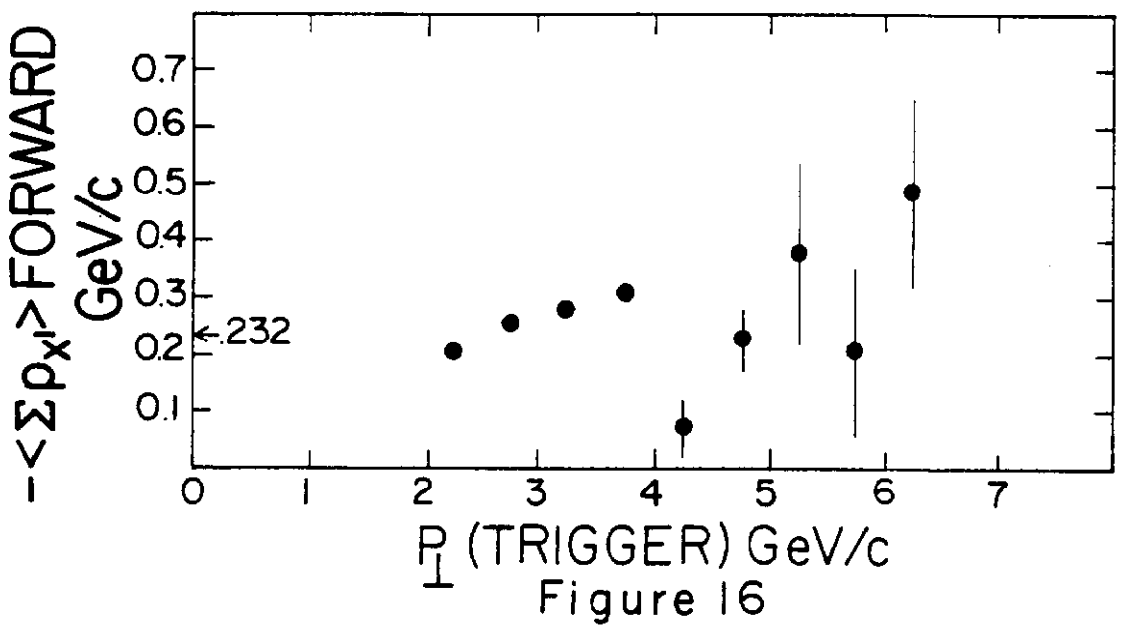

Figure 16

V. JET STRUCTURE

We define the jet fragmentation variables:

$$\left.\begin{aligned} \text{trigger:} \quad z &= \frac{p_{x,i}}{p_{jet}} \\ \text{away:} \quad z &= -\frac{p_{x,i}}{p_{jet}} \end{aligned}\right\} \text{ in the transverse plane}$$

P_i are the momenta of individual charged particles: p_{jet} is the total transverse momentum of the trigger jet including neutrals. An important advantage of this experiment over those not having magnetic analysis of the charged particles is that the momentum is determined more precisely at low-z (in contrast to the energy found from calorimeter pulse heights); low-z contributes a large part of the jet cross-section. However at values of $z < 0.20$ the magnetic field reduces the acceptance for charged particles. This region contains both our major losses and our main background of unwanted particles. These effects have been studied carefully in our analysis of the Be target[6] and we summarize from that paper.

A jet is a collection of particles whose vector sum leads to large p_t. So far, we have used in the sum all the particles, and only those particles, that enter the calorimeter. In comparing our cross-section with any theoretical model, one must ask if this choice is reasonable. As discussed above, we may have either omitted jet associated particles that miss the calorimeter, and/or included non-jet "background" particles that happen to be in the region of phase space subtended by the calorimeter. If all the particles in a jet had p_t's substantially larger than the "background", there would not be a problem. Unfortunately, our jets are a collection of low to moderate p_t particles. The good agreement of our z distributions with those from lepton processes indicates that the latter see a similar type of jet. We can get a feeling for the number of unwanted particles from the number of particles in the calorimeter for single high p_t triggers; we find one additional charged particle per event. This is an upper bound on the background because we expect some contribution to calorimeter multiplicity from the remaining fragments of the jet that produced the single particle high p_t trigger. One estimates a similar background when one looks at the calorimeter on the away side and subtracts off the away side jet (assuming it has the same multiplicity as the tri ger jet).

The difficult region, $z < 0.2$, contributes most of the charged multiplicity, i.e., 2.15 per event out of a total jet charged multiplicity of 3.17 for $4 < p_t^{jet} < 5$ GeV/c. However, it only contributes 15% of the jet p_t. So whatever way we treat this region will not alter our jet cross-section conclusions. In fact, comparison with lepton data[2] suggests that our z distribution is really quite sensible down to $z = 0$. Thus, to some extent, our problems have cancelled, i.e., we have lost roughly as many jet members as we have accepted background. SPEAR jets have a charged multiplicity of 2.5 for $p = 4$ GeV/c. We see a comparable value (2.74) after removing the obviously irrelevant particles with $p_{x'} < 0$. Our multiplicity still contains ~.5 background charged particles per event and as discussed above, summarizing from the Be paper,[6] this is roughly compensated by the same number of lost jet members.

The newly analyzed data from the hydrogen target are shown in Fig. 17.

If the jets observed in E-260 arise from the fragmentation of a quark and if quarks cascade into hadrons in a universal manner then the z distribution on the trigger side should be similar to that observed in e^+e^- or lepton produced jets. As was already seen in the analysis of the Be data these distributions do in fact look similar. The slight difference with the Be data for $z < 0.1$ is probably due to differences in track finding. The steeper away side is interpreted in the hard scattering picture as caused by Fermi motion of the partons in the incident hadrons.

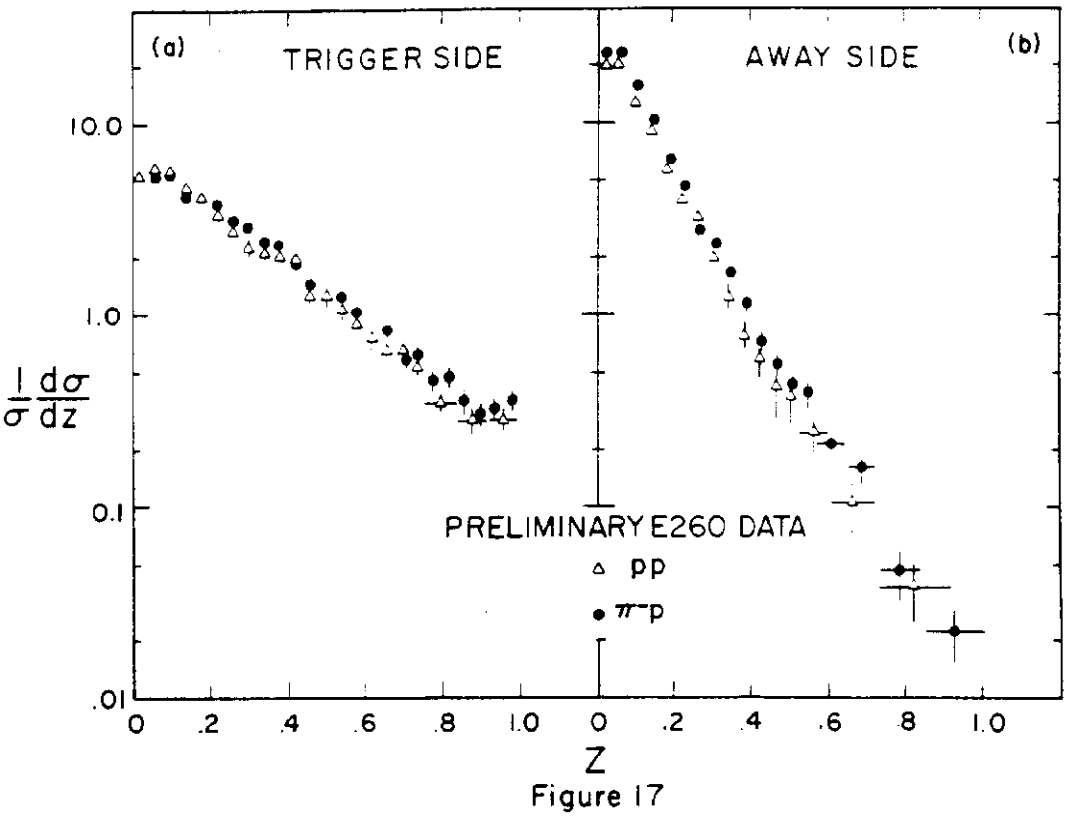

Figure 17

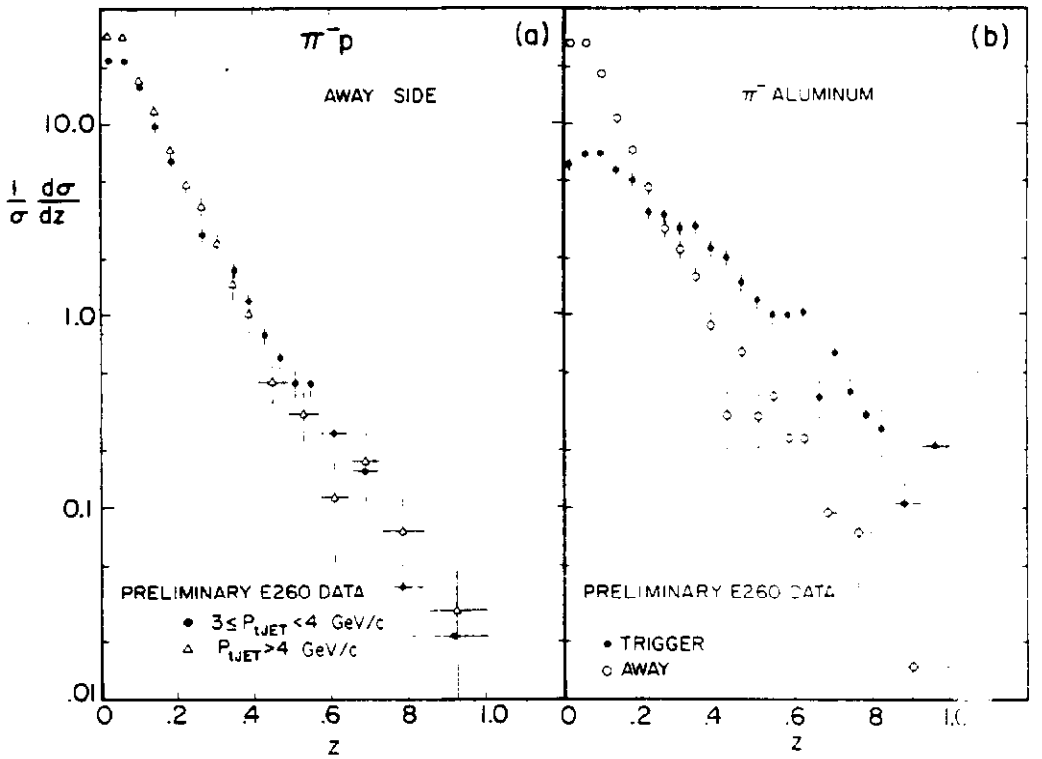

FIGURE 18

Does the away side scale? Figure 18a shows the away side z distribution for two different p_t jet cuts and as was observed in the Be data[b] there is a small departure from scaling. Are there nuclear effects? There does not appear to be a nuclear effect on the z-distribution. Figure 18b shows that jets produced from aluminum have a similar distribution in z as those produced from hydrogen.

Figure 19a shows the away side z-distribution for the single particle trigger data. The similarity of this distribution to the away side z-distribution for jet trigger events has been interpreted as support for the quark-quark scattering model and against a naive version of the constituent-interchange model.

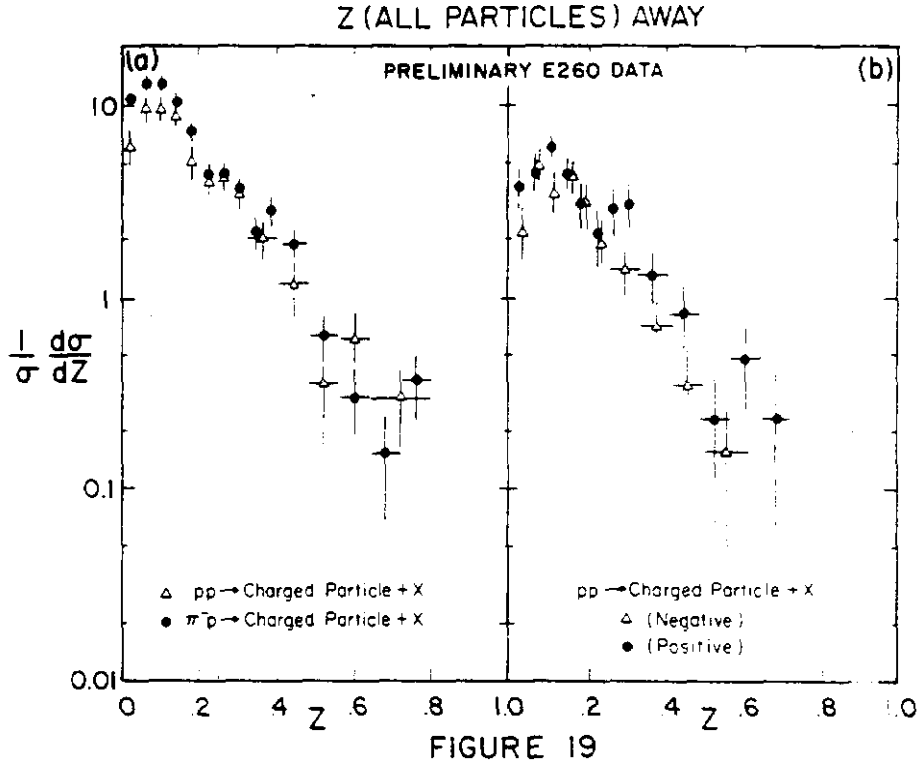

FIGURE 19

Table III summarizes $\bar{Q}$, the average charge for various conditions.

TABLE III

AVERAGE CHARGE

Trigger	Bias	Beam	T	A
Jet	> 4 GeV/c	π^-	.00 ± .01	.00 ± .01
		π^+	.32 ± .04	.10 ± .03
		p	.27 ± .01	.13 ± .01
Single	> 2 GeV/c	π^-	.10 ± .04	-.03 ± .05
		p	.35 ± .11	.17 ± .10

The numbers in the table are suggestive of the quark model but are subject to systematic errors still being investigated. In comparing the trigger and away side one should keep in mind that the kinematic cuts and the experimental acceptances are different.

We compare the away side z-distributions in Fig. 19b for positive and negative particles produced in pp collisions and note that the positive excess appears at all values of z but is greater at high z.

VI. CROSS-SECTION

The invariant cross-section is calculated using:

$$E\frac{d^3\sigma}{d^3p} = \left(\frac{1}{2\rho_t}\frac{dN}{dp_t}\right)\left(\frac{1}{\pi}\frac{1}{\Delta Y}\frac{1}{\Delta\phi}\right)\left(\frac{\text{DEAD TIME CORR}}{tF}\right) \times \left(\frac{C_{GEOM}}{\epsilon_{VERT}}\right)\left(\frac{1}{\text{BEAM COMP}}\right)$$

where t is the target thickness and F is the beam flux. We estimate the vertex efficiency for true events in H_2 or Al, ϵ_{vert} = (92 ± 3)%. The beam composition is given by 4 Cerenkov counters and for 200$^-$ GeV, π^- (96 ± 2)% and for 200$^+$ GeV, p (83 ± 2)% and π^+ (15 ± 2)%. The dead time correction depends on beam intensity and ranges between 1.3-1.5 with a small error. The fiducial cuts in y and ϕ are shown in Fig. 20. The geometric correction, C_{GEOM}, is found by assuming that the true distribution of jet vectors is uniform in y and ϕ within the fiducial area and is indicated by the dotted line. The correction used is independent of p_{jet}.

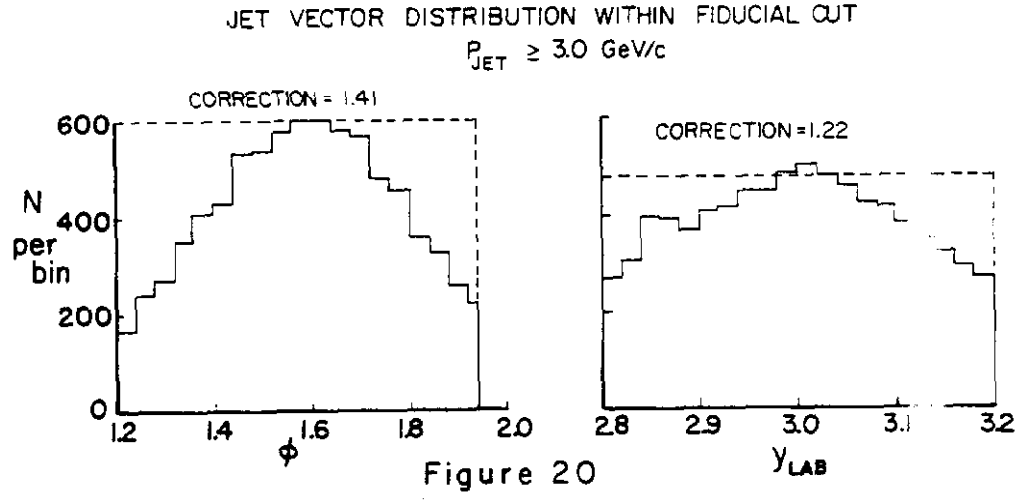

Figure 20

This fiducial cut results in a distribution of jet vectors in x and y on the face of the triggering calorimeter shown in Fig. 21. The smearing due to the magnetic field is apparent.

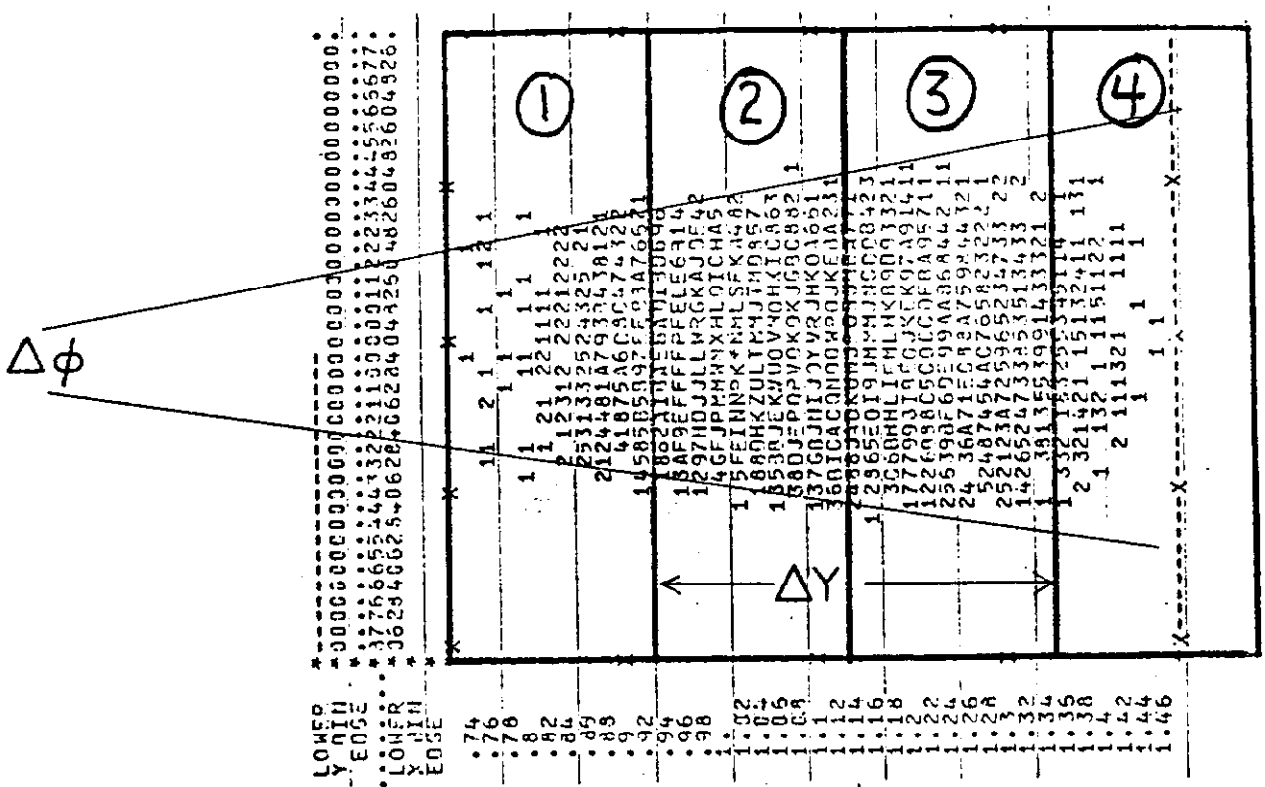

Figure 21

The single particle fiducial cut is a spatial cut in x and y on the face of the calorimeter shown in Fig. 22 and the corresponding $\Delta y \Delta \phi$ used in the cross-section calculation. The single particle threshold is smeared by the large ϕ acceptance.

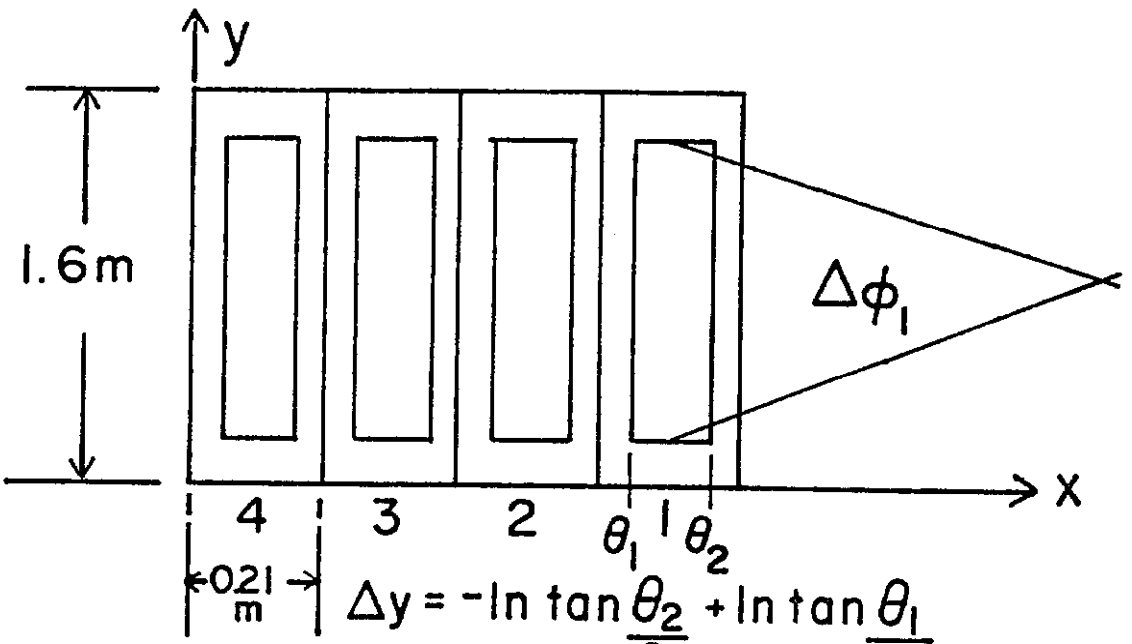

Figure 22

As was the case for our Be analysis we test our experiment against the accurate single particle data of the Chicago-Princeton group.[11] In Fig. 23 we plot our combined 2 and 3 GeV/c bias single particle trigger data. At high p_t where they are not affected by the trigger bias they agree with Chicago-Princeton cross-sections and at 2 GeV/c, are about 50% low, due to the calorimeter trigger threshold effect.

Also shown on Fig. 23 is the single particle distribution derived from the combined 3 and 4 GeV/c bias jet trigger data. These differ by ~15% due to normalization uncertainties which we will discuss below.

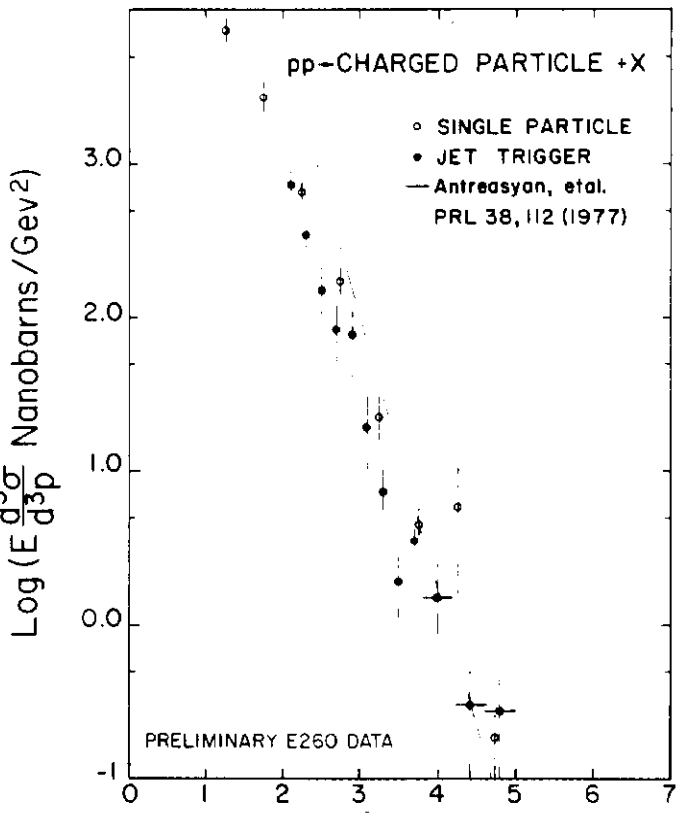

FIGURE 23

Jet-Cross-Sections

Next we look at the inclusive jet cross-section. Figure 24 shows the magnitude and p_t dependence of the various components of the jet for $\pi^- p \rightarrow$ Jet + X. The lines connecting the points are simply to guide the eye. Also shown is the prediction of Feynman, Field and Fox.[4] Over the p_t range shown (3-7 GeV/c) each of these components contribute an approximately constant fraction of the total cross-section. This is shown more clearly in Fig. 25 where the mean fraction (mean z) of the total jet p_t carried by each component is shown as a function

of p_t (jet). Figure 25 (a) includes data where p_t jet is allowed to be below the physical threshold (3 GeV/c and 4 GeV/c combined) whereas data in Fig. 25 (b) are required to be above threshold.

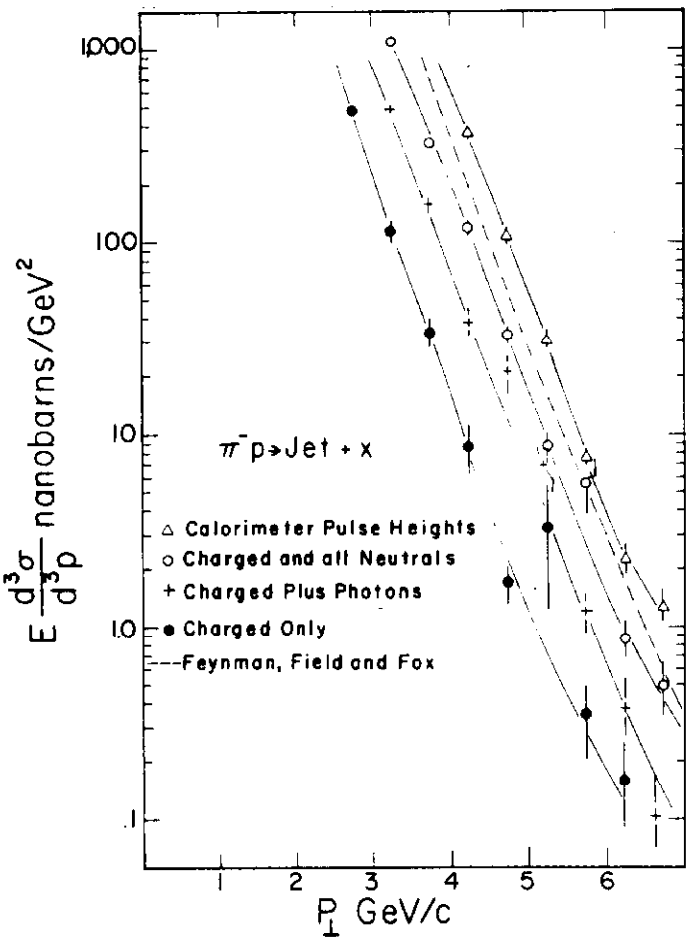

Figure 24

As seen in Fig. 25b, when we require the analyzed jet to be above the trigger threshold, (usually not the case) the fraction of neutral energy is considerably larger. This is because the magnetic field on the average adds a positive contribution to the p_t of the charged particles thus allowing predominantly charged events that are below threshold to trigger much more frequently than predominantly neutral events. A hadronic neutral component of 30% is, in all probability, too high, but, because this distribution is significantly different than those

in the Be data, we have not carried that analysis over directly. A more careful study of the hadronic neutrals awaits the re-analyzed H_2 data set. In the meantime, we take this hadronic neutral contribution at face value, without applying any of the reduction techniques used in the Be paper. This may make a factor of about 1.5 overestimate of the cross-sections.

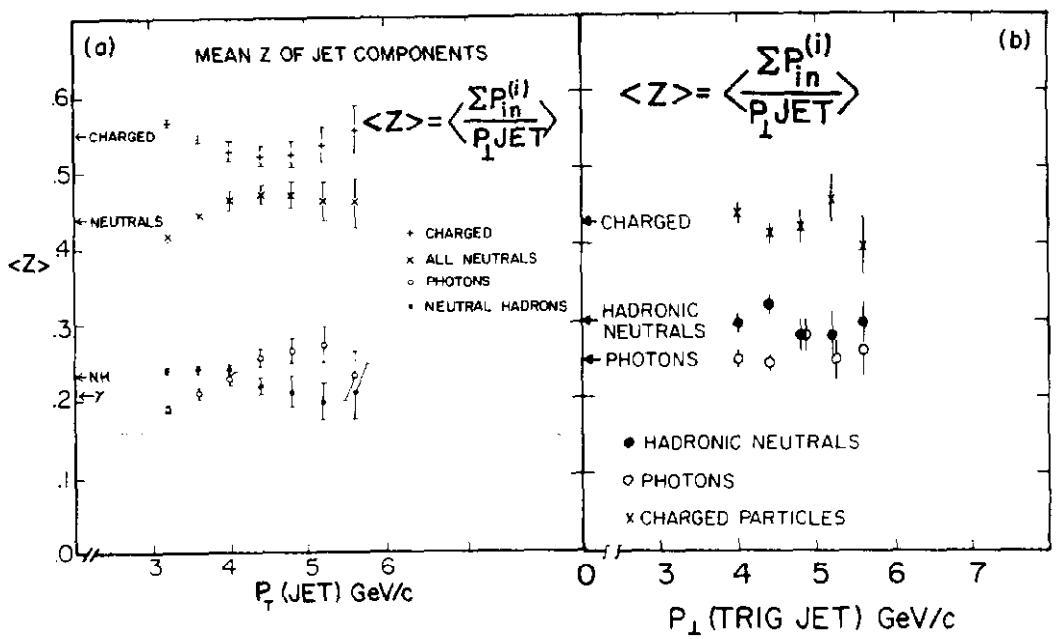

Figure 25

Figure 26 shows the pp and $\pi^- p \rightarrow$ Jet + X cross-sections. These cross-sections include data taken at 3 GeV/c and 4 GeV/c trigger biases as well as a sample of unbiased data. The unbiased data sample is analyzed in the same way as the jet trigger data, i.e., it has the same acceptance corrections, fiducial cuts, etc. However, it is somewhat different in that there are no threshold effects in the calorimeter. This shows up in that the calorimeter pulse height spectrum is much closer to the final jet p_t spectrum than is the case for the jet trigger data (Fig. 24). We have imposed a $p_t \geq 1.0$ GeV/c software cut on the unbiased data. Superimposed are the predictions of Feynman, Field

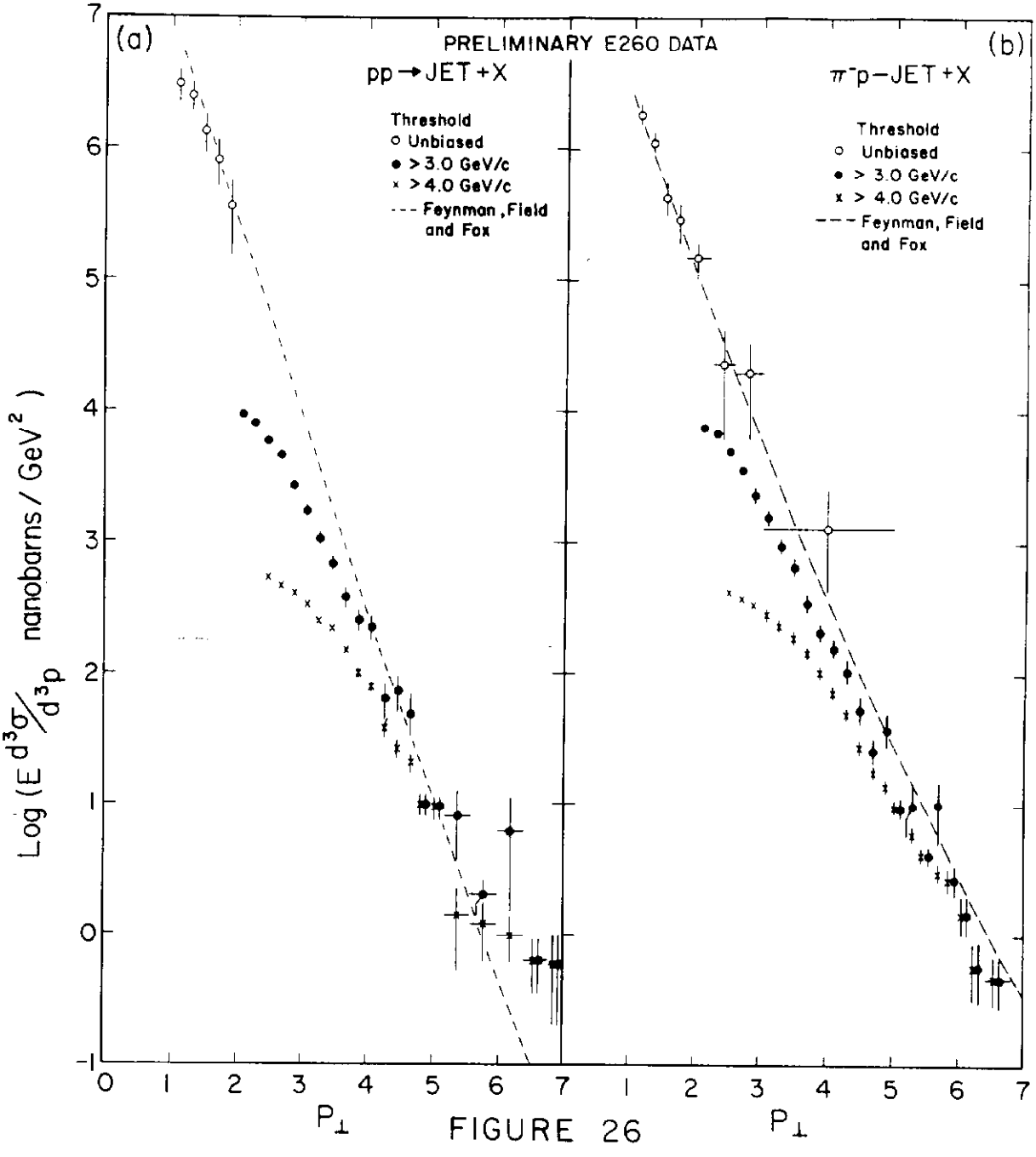
PRELIMINARY E260 DATA
(a)
pp → JET + X
Threshold
○ Unbiased
● > 3.0 GeV/c
× > 4.0 GeV/c
--- Feynman, Field and Fox
(b)
π⁻p → JET + X
Threshold
○ Unbiased
● > 3.0 GeV/c
× > 4.0 GeV/c
--- Feynman, Field and Fox
Log (E d³σ/d³p nanobarns / GeV²)
P⊥
P⊥

FIGURE 26

and Fox.[4] We observe that, as previously published,[6] the jet cross-sections are at least 100 times the charged particle inclusive cross-sections. Also we observe that the data is in quite good agreement with the predictions.

Before comparing the πp and pp cross-sections in detail, a word must be said about the various systematic and background effects in this analysis. First, we are at present unable to completely eliminate background events (such as correlated halo) which are expected to be roughly flat in p_t and hence show up strongly at the highest p_t's. Such effects are intensity dependent and, because our positive beam data were taken at 30 to 50% higher intensity than the negative beam data, effect the shape of the π and p spectra differently. This background is thought to be significant above $p_t \geq 6$ GeV/c. In addition, there are systematic uncertainties in the overall absolute normalizations of πp and pp data of the order of 20%, as well as somewhat smaller uncertainties in the internal normalizations (e.g., low bias to high bias, etc.). The largest systematic effects will only effect the magnitude, but not the shape of cross-sections and cross-section ratios.

With this caveat, we show the proton to pion ratios. Figure 27a exhibits the well-known results of the BNL-Caltech-LBL experiment showing that pions become more effective than protons in producing π^o's as x_t (π^o) increases. The curve is the prediction of Field and Feynman.[4] The ratio of our charged single particle cross-sections is shown in Fig. 27b, again with the predicted curve. Although our data lie quite low in comparison, the same

trend is shown quite strongly. We are sufficiently uncertain about the overall normalization that we are not prepared to claim a disagreement with the prediction.

The ratio of cross-sections for proton and pion induced jets in Fig. 28a shows a similar trend, but appears to be significantly flatter in x_t. At low x_t are two interacting beam points, which although they have large statistical errors, agree with the ratio of total cross-sections. Also shown is the prediction of Feynman, Field and Fox[4] for jet production. This curve is very similar in shape to the prediction for π^o's, but is shifted to higher x_t by about 1/2 unit. This shift is due in the model to the parent-daughter relationship of jets to high p_t particles. The detailed shape of the predicted curve depends heavily on the relatively unknown pion structure functions and thus can probably accomodate a fair range in the data without breaking down. Our data qualitatively support this idea, but are subject to large systematic uncertainties and so as yet cannot be claimed to disagree in detail.

Figure 28b shows the cross-section ratios for jet production on aluminum. These points, though having large statistical errors, are very well normalized to the corresponding H_2 cross-sections. We see that there is a significant shift to higher x_t. This might be explained by some nuclear rescattering mechanism which effectively gives the jet an extra GeV/c of p_t on the average.

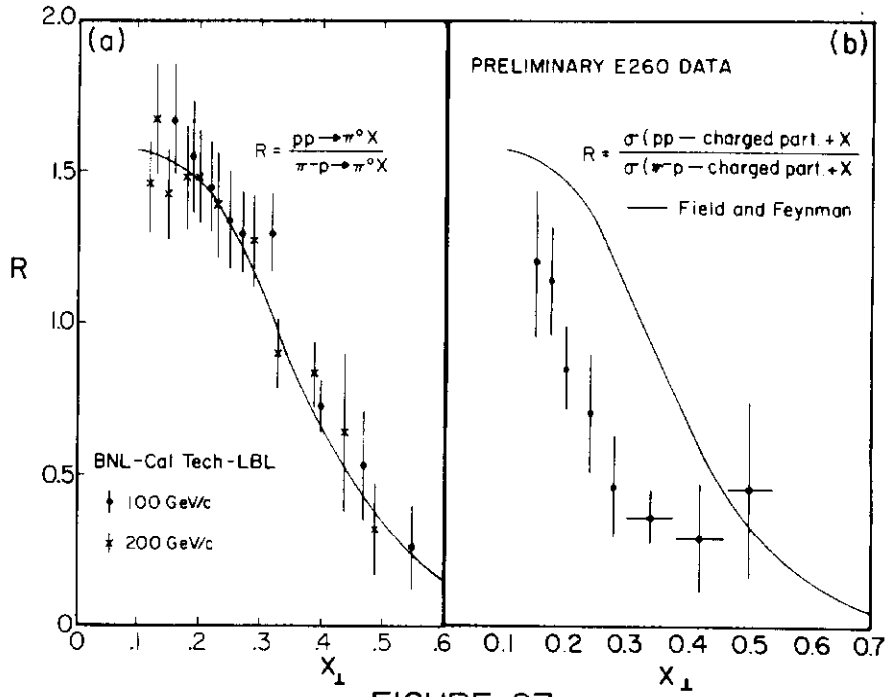

FIGURE 27

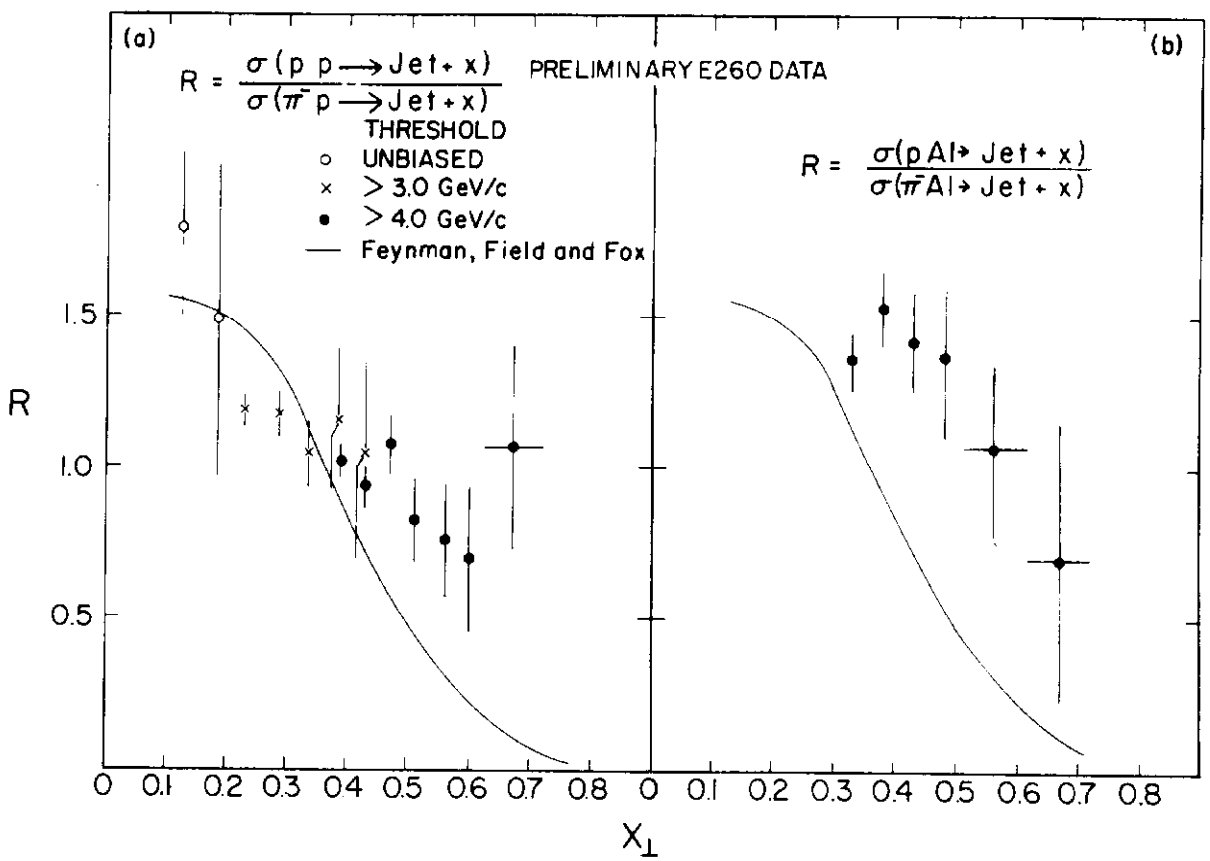

Figure 28

The A-dependence of the cross-section, parameterized as A^{α} and determined with only A = 1 and 26, is shown in Fig. 29a for single particles and in Fig. 29b for jets.

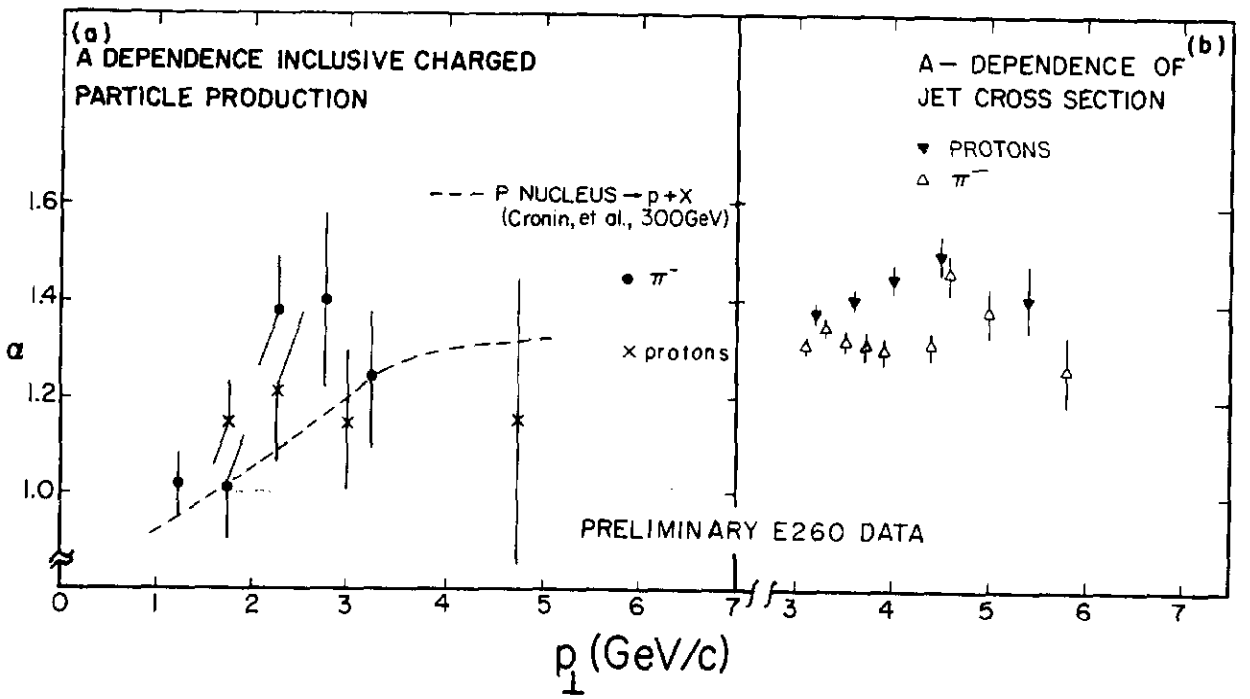

Figure 29

The A-dependence of the cross-section for pN → single particle + X is in agreement with the results of the Chicago-Princeton collaboration[14] but the errors are too large to draw any conclusions on the pion-proton comparison. On the other hand the jet A-dependence seems to be stronger for protons than pions. This may be entirely unrelated to the production of different types of hadrons but it is interesting in looking at Fig. 29 to recall that the Chicago-Princeton group[14] find $\alpha \simeq 1.1$ for $pN \to \pi^{\pm}X$ and $\alpha \simeq 1.3$ for $pN \to p^{\pm}X$.

VII. CONCLUSIONS

1) We have shown that emperically defined jets at low p_t (our unbiased data) do not show statistically significant coplanarity. This is consistent with the negative results of a search for alignment in high energy collisions using bubble chamber data.[15] But as p_t increases, jet trigger events become progressively more coplanar.

2) The jets in our data have a fragmentation distribution in agreement with lepton-hadron and e^+e^- induced jets.

3) The jet/single particle ratio is large ($\gtrsim$ 100).

4) The away side z-distribution is similar for jets and single particle triggers.[6]

5) The p/π ratio decreases with increasing x_t for both jets and charged single particles.

6) There is a strong A-dependence to jet production. If it is parameterized as A^α then $\alpha(\pi^-$ incident) $\simeq$1.3, and α(p incident) $\simeq$ 1.45 and roughly constant with p_t (3-6 GeV/c).

If statistical fluctuations were the cause of our jets then the p/π ratio would equal the ratio of the total inelastic proton and pion cross-sections or about 1.5 and the A-dependence would be characteristic of low p_t scattering ($\alpha < 1.0$). Thus the falling value of p/π and the large value of α are strong evidence for new dynamics.

These observations taken collectively are strong evidence that jets exist and as shown in our previous work[6] are not simply single particles combining statistically to give high p_t, but are a phenomenon due to a short range correlation between the particles comprising the jet and a manifestation of the underlying dynamics of the high p_t hadron-hadron interaction.

ACKNOWLEDGEMENTS

We are grateful for the support given us in running this experiment by the staffs of the Accelerator Division, the Meson Department, and the Research Services Department at Fermilab.

REFERENCES

*Work supported in part by the U.S. Energy Research and Development Administration under Contracts No. E(11-1)-68 (Caltech) and E(11-1)-2009 (Indiana); and the National Science Foundation under Grants No. PHY-76-80660 (UCLA) and PHY-73-04640 (Illinois).

†Permanently at the Max Planck Institute fur Physik and Astrophysik, Munich, Germany.

††Present Address: Oak Ridge National Laboratory, Oak Ridge, Tennessee.

†††Present address: California Institute of Technology, Pasadena, California.

[1]B. Alper et al., Phys. Lett. 44B, 521 (1973).

M. Banner et al., Phys. Lett. 44B, 537 (1973).

F. W. Büsser et al., Phys. Lett. 46B, 471 (1973).

[2] G. Hanson et al., Phys. Rev. Lett. 35, 196 (1975).

[3] M. Della Negra et al., Nucl. Phys. B104, 429 (1976).

"Observation of Jet Structure in High p_t Events at the ISR and the Importance of Parton Transverse Momentum", M. Della Negra et al., CERN/EP/PHYS-77-10. March 25, 1977. "Preliminary Results from CERN Experiment R413" (British-French-Scandinavian collaboration). R. Møller, contribution to the VII International Colloquium on Multiparticle Reactions, Tutzing, Germany, June, 1976. See also "Large Transverse Momentum Phonemena", ISR Discussion Meeting no. 21, March 7, 1977. (M. Jacob, Editor).

[4] "Quark Elastic Scattering as a Source of High Transverse Momentum Mesons", R. D. Field and R. P. Feynman. Phys. Rev. D15, 2590 (1977).

"Correlations Among Particles and Jets Produced with Large Transverse Momenta", R. P. Feynman, R. D. Field, and G. C. Fox, CALT-68-595 (1977).

[5] D. Sivers, S. J. Brodsky, and R. Blankenbeckler, Phys. Reports 23C, 1 (1976). "Large p_t Physics: Data and Constituent Models", S. D. Ellis and R. Stroynowski, SLAC-PUB-1903, March, 1977.

[6] C. Bromberg et al., Phys. Rev. Lett. 38, 1447 (1977). "Production of Jets and Single Particles at High p_t in 200 GeV Hadron-Beryllium Collisions", C. Bromberg et al. Publication in preparation.

[7] More details can be found in "Multiparticle Spectrometer at

Fermilab", A. Dzierba, E. Malamud, and D. McLeod, unpublished report, March, 1977.

[8]"The M6 Beam Line", E. Malamud, unpublished report, February 2, 1977.

[9]"Multiparticle Spectrometer Calorimeters", H. Haggerty, Proceedings of the Calorimeter Workshop, p. 251, Fermilab, May, 1975.

[10]G. Charlton et al., Phys. Rev. Lett. 29, 515 (1972).

[11]D. Antreasyan et al., Phys. Rev. Lett. 38, 112 (1977).

[12]"High p_t and Jets - Theory". G. C. Fox, Proceedings of the Meeting of the Division of Particles and Fields, Brookhaven BNL-50598, 1976.

[13]G. Donaldson et al., Phys. Rev. Lett. 36, 1110 (1976).

[14]"High p_t and Jets - Experiment", H. J. Frisch, Proceedings of the Meeting of the Division of Particles and Fields, Brookhaven, BNL-50598, 1976.

[15]R. G. Glasser et al., Phys. Lett. 53B, 387 (1974).